ACS EARTH AND SPACE CHEMISTRY

http://pubs.acs.org/journal/aesccq

Article

Gas-Particle Partitioning and SOA Yields of Organonitrate Products from NO_3-Initiated Oxidation of Isoprene under Varied Chemical Regimes

Bellamy Brownwood, Avtandil Turdziladze, Thorsten Hohaus, Rongrong Wu, Thomas F. Mentel, Philip T. M. Carlsson, Epameinondas Tsiligiannis, Mattias Hallquist, Stefanie Andres, Luisa Hantschke, David Reimer, Franz Rohrer, Ralf Tillmann, Benjamin Winter, Jonathan Liebmann, Steven S. Brown, Astrid Kiendler-Scharr, Anna Novelli, Hendrik Fuchs, and Juliane L. Fry*

Cite This: *ACS Earth Space Chem.* 2021, 5, 785−800

Read Online

ACCESS | Metrics & More | Article Recommendations | Supporting Information

ABSTRACT: Alkyl nitrate (AN) and secondary organic aerosol (SOA) from the reaction of nitrate radicals (NO_3) with isoprene were observed in the Simulation of Atmospheric PHotochemistry In a large Reaction (SAPHIR) chamber during the NO_3Isop campaign in August 2018. Based on 15 day-long experiments under various reaction conditions, we conclude that the reaction has a nominally unity molar AN yield (observed range 90 ± 40%) and an SOA mass yield of OA + organic nitrate aerosol of 13−15% (with ∼50 $\mu g\ m^{-3}$ inorganic seed aerosol and 2−5 $\mu g\ m^{-3}$ total organic aerosol). Isoprene (5−25 ppb) and oxidant (typically ∼100 ppb O_3 and 5−25 ppb NO_2) concentrations and aerosol composition (inorganic and organic coating) were varied while remaining close to ambient conditions, producing similar AN and SOA yields under all regimes. We observe the formation of dinitrates upon oxidation of the second double bond only once the isoprene precursor is fully consumed. We determine the bulk partitioning coefficient for ANs ($K_p \sim 10^{-3}\ m^3\ \mu g^{-1}$), indicating an average volatility corresponding to a C_5 hydroxy hydroperoxy nitrate.

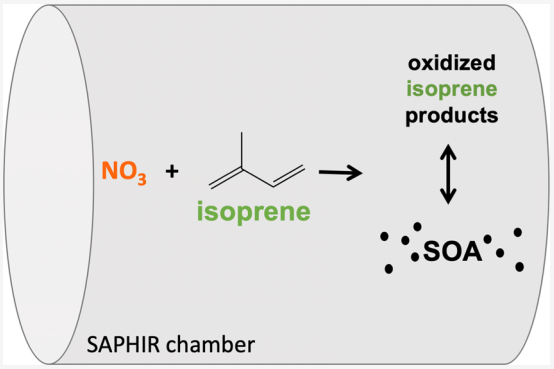

KEYWORDS: *isoprene, nitrate, oxidation mechanism, peroxy radicals, gas-aerosol partitioning, secondary organic aerosol*

1. INTRODUCTION

Isoprene (C_5H_8) has the largest nonmethane biogenic volatile organic compound emission, at around 600 Tg/year, compared to all other mono- and sesquiterpenes combined, which are emitted at around 150 Tg/year.[1] Isoprene is emitted during the day by deciduous trees[2] and is primarily oxidized by OH (daytime lifetime ∼ 1−2 h), O_3 (24 h average lifetime ∼ 1 days), and NO_3 (night-time lifetime highly variable, from 10 min to >100 h depending on available NO_x). During the day, OH and O_3 are the primary oxidizers; however, isoprene emissions are large enough that isoprene can remain abundant in the boundary layer[3] and can continue to react at night by O_3 and NO_3. Nitrate radical oxidation is considered night-time reaction because NO_3 reacts rapidly with photochemically generated NO and undergoes photolysis during the day;[4] however, due to its high reactivity with isoprene (rate constants of isoprene with O_3: 1×10^{-17} $cm^3\ molecules^{-1}\ s^{-1}$[5] and NO_3: 6.78×10^{-13} $cm^3\ molecules^{-1}\ s^{-1}$,[6] at 298 K), this reaction can also be important in power plant plumes[7] and shaded forest canopies where photolysis is suppressed. Because of this, NO_3 is an important oxidizer of isoprene, particularly in regions where urban or industry plumes travel into forests.

The nitrate (NO_3) radical-initiated oxidation of isoprene is a key atmospheric reaction in regions subject to both biogenic and anthropogenic emissions. Recently, several studies have shown large but variable mass yields of secondary organic aerosol (SOA) formed from this reaction, ranging from 2 to 14% in chambers[8,9] up to 30% based on field measurements,[10] suggesting that it may also be an important contributor to global aerosol concentrations.[11] This variability has spurred further research into the product branching ratios and volatility.[12,13] Even with generally lower SOA mass yields than the larger mono- and sesquiterpenes,[1] isoprene is

Received: November 16, 2020
Revised: February 17, 2021
Accepted: February 25, 2021
Published: March 11, 2021

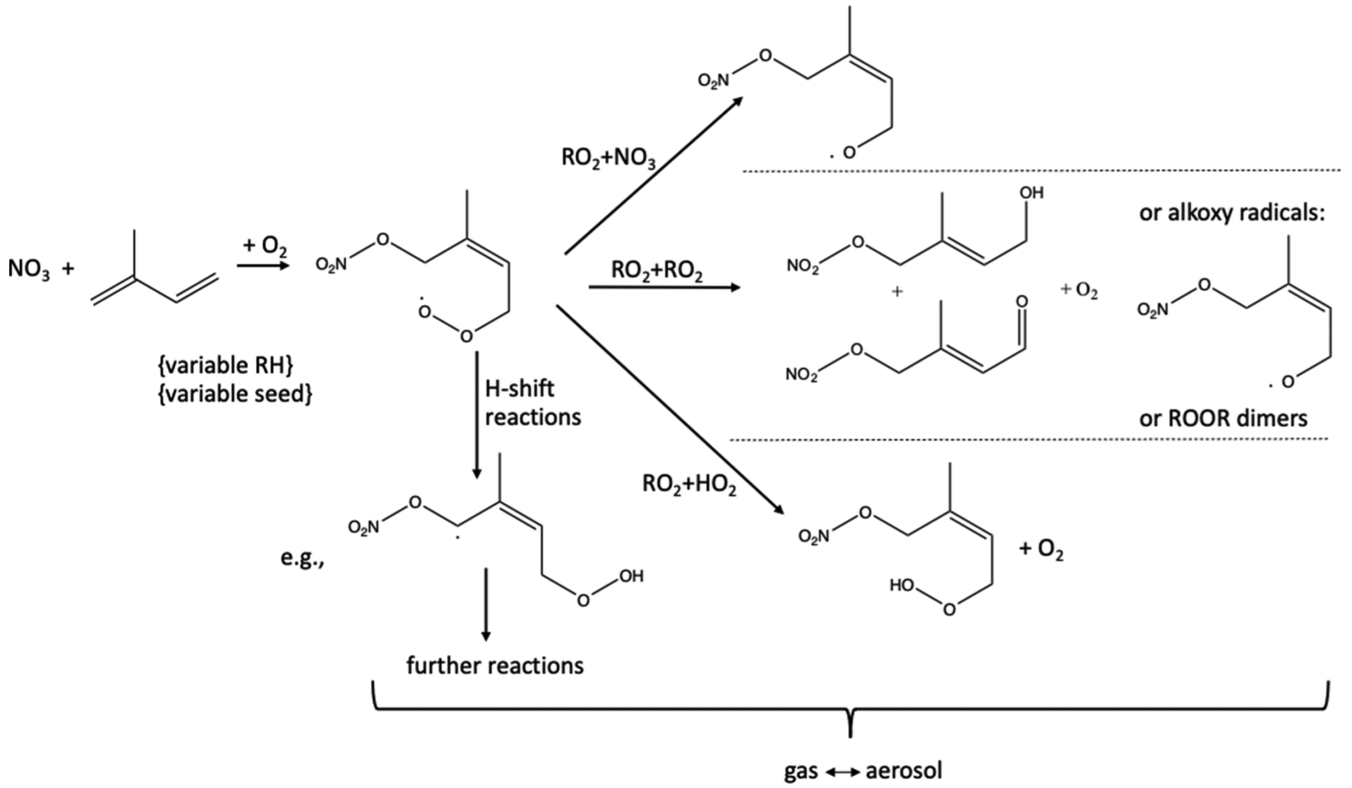

Figure 1. NO_3 + isoprene reactions, showing the major initial pathways of RO_2 reaction. This study explored varying RO_2 fate regimes, seed composition, and RH.

expected to be a substantial contributor to aerosol loading because of its far larger global emission rate.[14] More quantitative information about these NO_3-initiated isoprene oxidation products is necessary to better understand the mechanisms of these reactions for use in modeling and predictions of changes in the global aerosol budget. This knowledge will further improve our understanding of the impacts of SOA on solar radiative forcing and thus surface temperature,[15,16] visibility degradation, and human health.[17,18]

The importance of isoprene in the global SOA budget has been studied and reviewed recently.[14,19] The gas-phase products of isoprene photo-oxidation have previously been thought to be too small and too volatile to self-nucleate and condense into the particle phase, and studies have shown the total isoprene SOA mass yield for all oxidants to be ∼3%.[20,21] A chamber study on isoprene photo-oxidation by Liu et al.[22] found SOA mass yields up to 15%, a factor of 2 or more higher than mass yields used in chemical models. In the presence of seed aerosol, the organonitrate products from the oxidation of isoprene partition into the particle phase. The type of seed aerosol used (acidic/neutral or inorganic/organic) has also been shown to yield different amounts of SOA for the oxidation of isoprene.[23]

Atmospheric simulation experiments in chambers are valuable tools to investigate mechanistic details of VOC oxidation and SOA formation. In a large chamber such as the SAPHIR chamber used here (270 m^3 volume), a further advantage is the ability to access near-ambient conditions, because wall losses compete less efficiently with the chemical processes of interest. However, chamber studies do have limitations that must be considered in analyzing results. Most chamber studies of isoprene SOA show low amounts of oxidation products and especially low amounts of aerosol. One factor that may contribute to this is the insufficient time to allow products to further react after first-generation products have been formed. Due to the semivolatile nature of the SOA, products form and can quickly partition to the walls in a chamber, reducing the accessible reaction timescale. In the real atmosphere, reaction products continue to react much longer and can slowly form later-generation products; these products would normally only be formed quickly enough to be observed on chamber experiment timescales when run at elevated concentrations.

In the experiments reported here, to further simulate true atmospheric conditions and enhance partitioning to particles rather than walls, seed aerosol was used in some experiments. Beyond overcoming wall loss constraints, this use of seed aerosol is more similar to real atmospheric conditions, where a variety of different particles exist that isoprene gas products can condense onto. To the extent that current models use SOA parameterizations primarily derived from experiments without seed aerosol, they may underestimate partitioning to the particulate phase and thus SOA yields.

This NO_3Isop chamber campaign sought to characterize the mechanisms and yields of SOA from the NO_3-radical-initiated oxidation of isoprene under varying conditions, with a motivating question of whether certain chemical regimes lead to larger SOA mass yields (see Figure 1). This paper describes (1) the alkyl nitrate (AN or $RONO_2$) molar yields for the entire campaign, across both seeded and unseeded experiments, (2) the SOA mass yield and bulk aerosol composition for all seeded experiments, and (3) the observed aggregate gas-particle partitioning coefficient (K_p) for all seeded experiments. The observed AN yields for the different peroxy radical (RO_2) loss pathways help to interpret the oxidation mechanism; we expect that under hydroperoxy (HO_2)-dominated bimolecular

https://dx.doi.org/10.1021/acsearthspacechem.0c00311
ACS Earth Space Chem. 2021, 5, 785−800

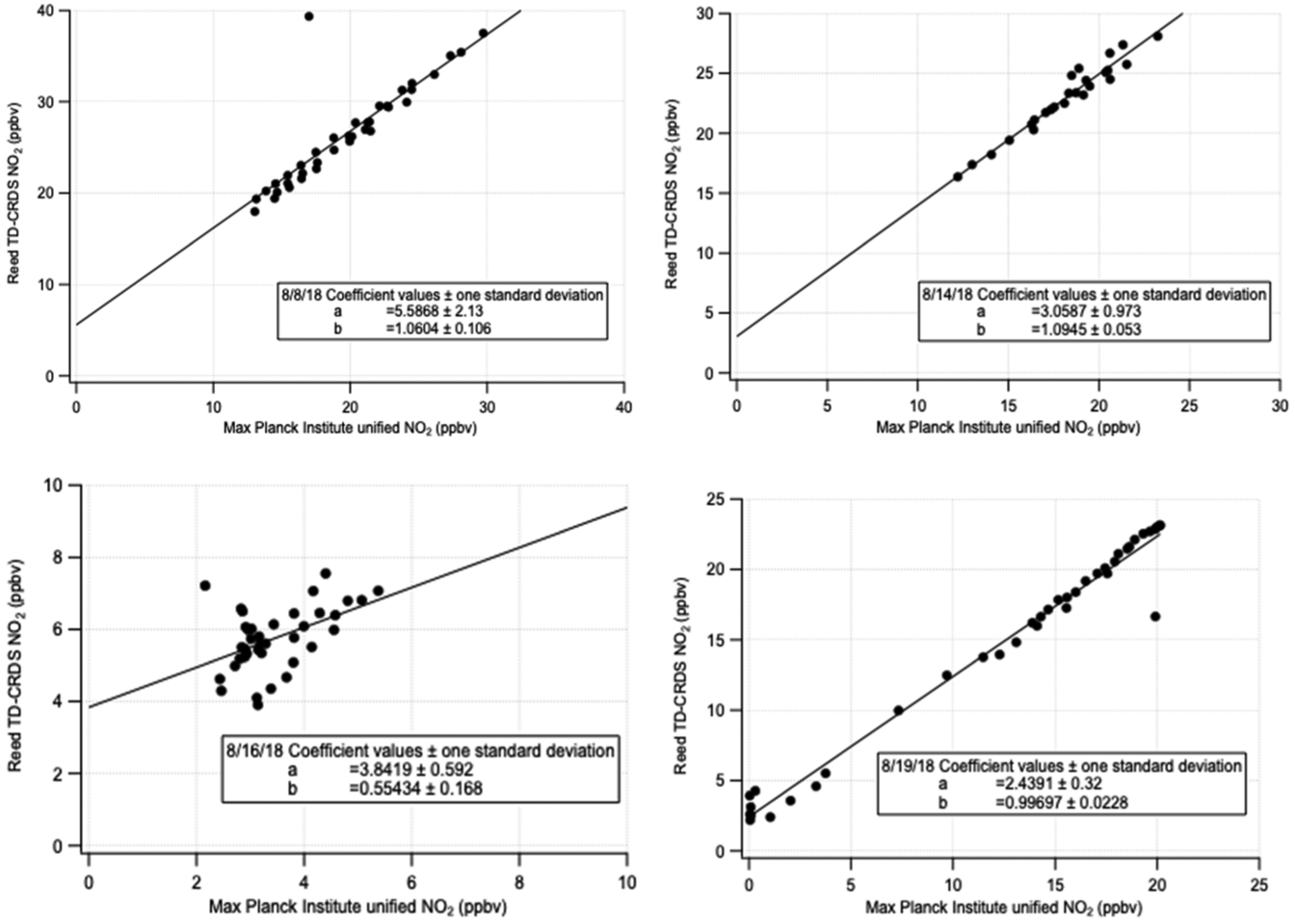

Figure 2. NO_2 comparisons from SAPHIR chamber experiments in Julich, Germany, in 2018 (experiments from 08 August, 14 August, 16 August, and 19 August). This figure shows illustrative scatter plots of the TD−CRDS NO_2 against the unified NO_2 data set from three independent Max Planck Institute run cavity ring-down measurements. These instruments have slightly varying relationships to one another day-to-day, suggesting the presence of inlet memory effects. Slopes were, for the most part, consistent within 10%, resulting in an estimated uncertainty of the AN measurements used here of 10%. Several days (August 9, 12, 16, and 21) had more scatter and thus poorly defined slopes with differences of up to 50%; these are indicated by italics in Table 1.

loss conditions, we will form more organic peroxides, while under RO_2-dominated bimolecular loss conditions, we will favor dimer formation, and under lower concentrations, we will favor unimolecular decomposition which could enable auto-oxidation via intramolecular H-shift reactions. On the other hand, the formation of an alkoxy radical (RO) is possible from all bimolecular reactions. The K_p can be compared to theoretical calculations of partition coefficients to estimate the functionality of the major products and can be compared to other experimentally derived partitioning coefficients to compare volatilities. Better understanding of the gas-particle partitioning and SOA yields can improve model predictions of global aerosol.

2. EXPERIMENTAL METHODS

2.1. SAPHIR Chamber Experiments. The SAPHIR chamber is a double-walled 250 μm-thick Teflon-FEP cylindrical cavity, 5 m in diameter and 18 m long with an approximate 270 m^3 volume. The chamber is operated with synthetic air, and chamber pressure is kept at 35 Pa (overpressure) above ambient pressure to avoid contamination from external air. The chamber is inside of an aluminum structure with maneuverable shutters that can be opened to simulate day time chemistry. Further description of the SAPHIR chamber can be found in other studies.[24,25] The campaign described here included 1 month of chamber experiments in August 2018.[26]

NO_3 was formed in these experiments by the reaction of NO_2 + O_3 and, in one case, from the dissociation of N_2O_5 supplied from a solid sample in a cold trap. In all experiments, NO_3 and NO_2 will exist in equilibrium with N_2O_5. Experiments for the NO_3Isop campaign were characterized by temperatures between 15 and 40 °C, most typically 20−25 °C, and under varying humidity conditions (ranging from 0 to 80% relative humidity). Ozone was injected to keep a chamber mixing ratio of approximately 100 ppbv, while the NO_2 and isoprene concentrations varied. NO_2 injections were varied to achieve mixing ratios of 5 to 25 ppbv. Isoprene was added in injections that achieved approximately 3 or 10 ppbv. Generally, O_3 and NO_2 were introduced at the same time and isoprene was added shortly after. This was repeated periodically throughout some experiments to continue buildup of products; the number of injections was not uniform across all experiments.

In experiments aiming to favor RO_2 + HO_2 reactions, an OH scavenger, usually carbon monoxide (CO), and an HO_2 source, propene (via ozonolysis), were added (09 August

https://dx.doi.org/10.1021/acsearthspacechem.0c00311
ACS Earth Space Chem. 2021, 5, 785−800

and 21 August). To favor RO_2 isomerization, isoprene and oxidant concentrations were kept lower to keep the concentration of the radicals low, so that RO_2 would be produced more slowly and would be more likely to undergo unimolecular reactions due to the lower concentrations of potential bimolecular reaction partners. This can be seen in experiments from 7 August, 10 August, 16 August, and 18 August. In an effort to favor RO_2 + RO_2, higher concentrations of isoprene were added to increase the RO_2 production rate, as on 08 August, 13 August, 14 August, 15 August, and 20 August. On 19 August, N_2O_5 was used as a NO_3 source to avoid any contribution from ozonolysis to an RO_2 + RO_2 regime experiment. Some experiments studied the night-to-day transition chemistry by opening the shutters after all reactants had been added. This transition can be seen in experiments from 6 August, 12 August, 16 August, and 18 August. A full list of experiments and experimental parameters can be found in the Supporting Information section in Table S1.

Seeded experiments also had the addition of ammonium sulfate seed before the oxidants were introduced. Typically, approximately 60 μg m^{-3} seed aerosol was added at the start of experiments before any gas-phase reagent additions. Ammonium sulfate was used as the inorganic seed compound, while some experiments also had β-caryophyllene and O_3 added to coat the seed with an organic coating produced from the rapid ozonolysis of caryophyllene. In these experiments, NO_3 production and isoprene oxidation were started only after β-caryophyllene had reacted away with ozone.

An overview of the instruments used for the analyses below is shown in Table S2, alongside key parameters for these experiments.

2.2. TD−CRDS Measurements at SAPHIR. We deployed a thermal dissociation−cavity ring-down spectrometer (TD−CRDS) for the measurements of NO_2, total peroxynitrates (ΣPNs), total alkyl nitrates (ΣANs), and HNO_3, in both the gas phase and particle phase. This instrument[27] couples a custom-built thermal dissociation oven inlet system with a commercial Los Gatos Research Inc. (model #907-0009) cavity ring-down spectrometer. To measure the various classes of organonitrates, the four inlet ovens are held at room temperature, 130, 385, and 700 °C.

At the SAPHIR chamber, the TD−CRDS was housed in one of the trailers beneath the chamber, with a 5 m-long 1/4" Teflon inlet line running through the floor into the chamber. This necessarily relatively long inlet line appears to have resulted in some inlet memory effects that were apparent in measurements during this chamber campaign. At the instrument flow of 1.2 lpm, this inlet length results in a residence time of 3.1 s in the line.

During the NO_3Isop campaign, TD−CRDS NO_2 measurements were compared to those from other instruments measuring NO_2. A unified NO_3Isop campaign NO_2 data set was created from NO_2 measurements from two independent custom-built thermal dissociation cavity ring-down NO_2 spectrometers operated by the Max Planck Institute.[28] This is used as the abscissa in Figure 2, which illustrates comparisons made for several illustrative days. The Reed TD−CRDS instrument typically measured higher values, exhibiting substantial and varying positive intercepts, suggesting background NO_2 from inlet memory effects. The corresponding NO_2 time-series comparisons for these four illustrative days are shown in the Supporting Information, Figure S1. The slopes of the intercomparison typically range from 1 to 1.1 but in some (especially low concentration) cases is much more poorly constrained due to high scatter. The four comparisons show that experiments spanning a large range of NO_2 mixing ratios have the best defined slopes. Only the slope variability is relevant to the uncertainty of the AN measurement, since it is a subtractive measurement and any varying NO_2 background will be removed. Based on these slope differences in multiple days' comparisons of independent measurements of NO_2 concentrations, we make the assessment that the uncertainty in ANs measured by TD−CRDS during these experiments is 10%, and we flag several experiments with more poorly defined NO_2 correlations as questionable and thus omit them from the overall AN yield calculation.

There are several corrections that can be applied to the data from the various measurement channels in the TD−CRDS:[27] denuder breakthrough of various species on the aerosol channels, radical recombination in the PAN oven, and O_3 pyrolysis in the HNO_3 oven. Because we are only using the gas-phase ΣANs measurement for this study, the data do not require corrections. The instrument was zeroed hourly (by diversion of the inlet to the CRDS through an NO_2 scrubber) during the campaign. This scrubber was baked immediately prior to the campaign to remove any potential background signal.

We note that the TD−CRDS instrument can, in principle, measure aerosol-phase organic nitrates. However, because only a small amount of produced ANs partitioned into the aerosol phase across all experiments and because a 5 m Teflon inlet line was required, which will transmit gas-phase ANs well but allow losses of particles, we found that aerosol-phase ANs were below the detection limit of TD−CRDS for this campaign. Therefore, as described below, we use the aerosol mass spectrometry (AMS) organic nitrate aerosol measurements. For these experiments, our singular focus on the ΣAN measurements obviates the need to make ozone pyrolysis or recombination or denuder breakthrough corrections. A representative AN thermogram (ramping oven temperature) on the SAPHIR chamber mix of isoprene + NO_3 products is shown in Supporting Information, Figure S2.

2.3. AN Yield Determination. ANs are predicted and observed to be the majority of products for the NO_3 radical-initiated oxidation of isoprene. To calculate the total AN yield for each experiment, a measurement of the total ANs (ΣANs) was used from a thermal dissociation−cavity ring-down spectrometer (TD−CRDS) and divided by the amount of isoprene consumed by NO_3 during the experiment. Wall loss corrections were applied to the ΣAN measurements, using a wall loss rate measured for ΣANs during a previous chamber study in the SAPHIR chamber (2.2×10^{-5} s^{-1}; Rollins et al.[9]). Unfortunately, we do not have an experimental determination of wall losses from this campaign period; using this older determined rate assumes that wall losses in the SAPHIR chamber do not change significantly over time. For the longest experiment, 10 August (~7 h), we can see that the maximum cumulative wall losses for these experiments would result in a final concentration corrected upward by 25%. The more typical 3 h experiments had a maximum wall-loss-corrected concentration difference of 7%.

The amount of isoprene that reacted with NO_3 was calculated using the measured isoprene loss (VOCUS, see Table S2) and subtracting from that the losses due to dilution and reaction with O_3. The VOCUS isoprene data were corrected with an empirical factor of 0.7 for the dry days, an

https://dx.doi.org/10.1021/acsearthspacechem.0c00311
ACS Earth Space Chem. 2021, 5, 785−800

adjustment based on comparison to another proton transfer reaction mass spectrometry used during this campaign, as well as the change in measured OH and NO_3 reactivity at the point in time at which isoprene was injected.[26] The dilution loss rate was derived from the measured inflow required to keep the chamber at constant pressure relative to the total chamber volume, and the loss to ozonolysis was calculated from the measured O_3 concentration using the IUPAC-recommended rate coefficient[29] $[1.05 \times 10^{-14} \times \exp(-2000/T)]$. Losses due to the reaction with OH are not included, since the OH concentration was below the limit of detection. The resulting amount of isoprene consumed by reaction with NO_3 remains an upper limit of the actual value, since the contribution of OH radicals could not be determined because their concentration was below the limit of detection. Instead, the given uncertainty (the larger of 10% or 0.5 ppbv) includes the amount of isoprene that would have been consumed, had the concentration of OH radicals been exactly at the detection limit. Further discussion of uncertainty propagation to the ANs and SOA yields is shown below in Sections 3.1 and 3.2.

The AN yields reported here represent the molar fraction of isoprene that reacted with NO_3 and subsequently produced an AN product. We assume negligible contributions from nitrates other than from NO_3 + isoprene; we note slightly larger AN yields under the RO_2 + HO_2 regime, suggesting that there may be some contribution from nitrates from NO_3 + propene (which was present in all HO_2 experiments; modeling suggests that approximately the same amount of propene as isoprene reacts with NO_3). The AN molar yield was calculated for each experiment day by determining the slope of the wall-loss-corrected measured AN concentrations versus the isoprene consumed by NO_3 (see Figure 3 for a representative example).

2.4. AMS Measurements and SOA Yield Calculations.

A high-resolution time-of-flight AMS (HR-ToF-AMS, Aerodyne Research Inc., USA) instrument was used to measure total mass concentrations and size distribution of nonrefractory chemical composition of the PM_1 (including ammonium (NH_4^+), nitrate (NO_3^-), sulfate (SO_4^{2-}), chloride (Cl^-), and organic compounds) inside the SAPHIR chamber. The high-resolution measurements were also used to determine and track the changes in the oxygen to carbon ratio (O:C) of the SOA during the cause of each experiment. Details of the instrument are described in previous publications.[30,31] Only instrument parameters and settings specific to this campaign will be given here. Two calibrations were performed (at the beginning and the end of the campaign) using size-selected 350 nm dried NH_4NO_3 particles and a condensation particle counter (CPC, model 3786, TSI, USA), as described in previous studies.[32] An average ionization efficiency of $(8.15 \pm 0.26) \times 10^{-8}$ was determined. Relative ionization efficiencies (RIE) for NH_4^+ and SO_4^{2-} were determined during the standard calibration procedures as well. The RIE of Org, NH_4^+, NO_3^-, SO_4^{2-}, and Cl^- were 1.4, (3.78 ± 0.12), 1.1, (1.13 ± 0.04), and 1.3, respectively. AMS collection efficiency was determined by comparing AMS and scanning mobility particle sizer (SMPS) data and was found to be ~0.5. Aerosol mass concentrations were corrected for wall losses using the decrease in the sulfate mass concentration of AMS. SO_4^{2-} originates only from the seed aerosols on which the products from the oxidation of isoprene will condense. Therefore, one can assume that the loss in aerosol due to dilution and wall loss can be corrected using SO_4^{2-} as an inert tracer for the loss processes in the chamber. Particulate organic nitrate mass

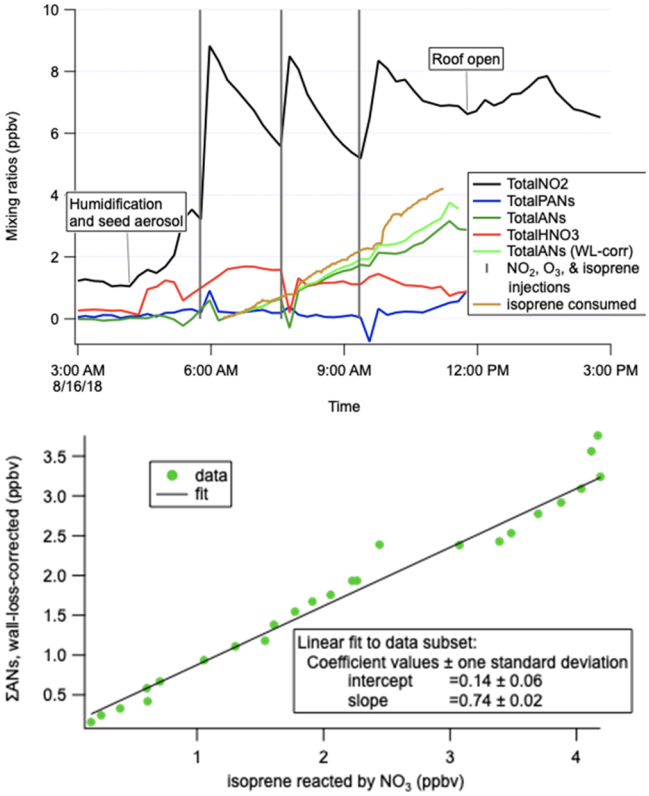

Figure 3. Representative example of AN molar yield calculation, using the experiment of 16 August. Wall-loss-corrected total AN concentration over the full time series of each experiment (including multiple isoprene, NO_2, and O_3 injections) is regressed against isoprene reacted; the slope is converted to % to be the yield. This plot shows a 74% molar yield.

concentrations ($pOrgNO_3$) were calculated using the approach of determining the ratio of the NO_2^+ to NO^+ ion signal, discussed in more detail below. The resulting mass loading of $OrgNO3_{part}$ refers only to the mass of the nitrate moiety, with the organic portion of the ANs detected as OA. To determine SOA yields, experiments were selected where after initiating the reaction and subsequent increase in the organic mass fraction on the seed aerosol, stable conditions were reached and no more increase in organic mass on the seed aerosol could be observed. An example for a typical experiment is shown in Figure 4.

The introduction of seed aerosol prior to the start of the oxidation leads to an increase not only in the sulfate mass concentration but also in the organic mass concentration. This increase is likely due to the repartitioning of organics from the Teflon foil of the chamber and condensing onto the seed aerosols. The amount of the organic background mass concentration was determined for each experiment prior to the start of the oxidation and considered to be constant and only affected by dilution and wall losses. The AMS organic mass concentration was corrected by subtracting the determined background concentration.

For these experiments, the SOA yields were calculated based on eq 1, using the background-corrected AMS mass concentrations, either the organic nitrate SOA ($\Delta SOA = \Delta OrgNO_{3part}$) or a combined organic and organic nitrate SOA ($\Delta SOA = \Delta OA + \Delta OrgNO_{3part,max}$) for the numerator, in both cases using the calculated isoprene consumed by NO_3 as the denominator ($\Delta isoprene$ = isoprene consumed by NO_3).

https://dx.doi.org/10.1021/acsearthspacechem.0c00311
ACS Earth Space Chem. 2021, 5, 785−800

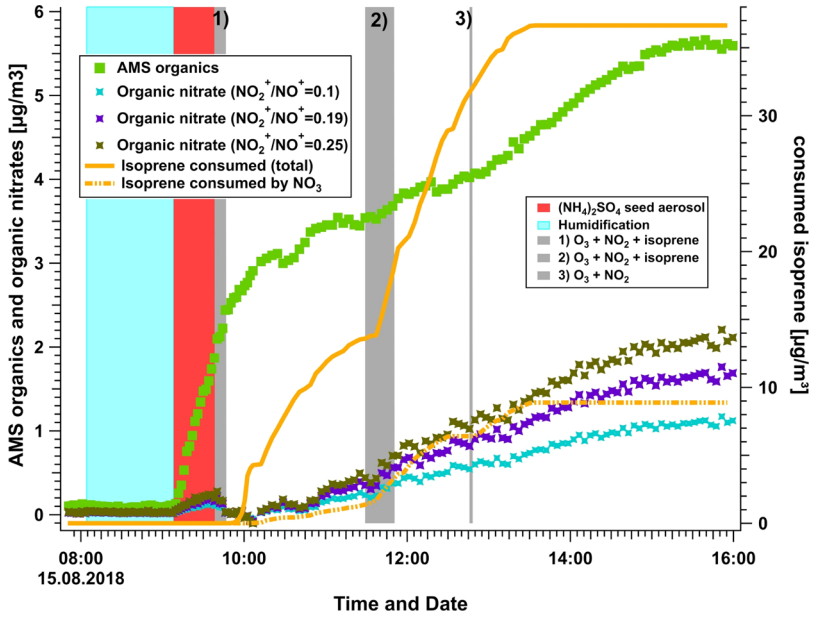

Figure 4. Time-series data for 15 August experiment, showing the AMS organics and calculated organic nitrates using different NO_2^+/NO^+ ion ratios on the left axis. The calculated isoprene consumed by NO_3 and total consumed isoprene are shown on the right axis. Colored bars indicate the start and duration of additions to the chamber such as water, seed aerosols, NO_2, O_3, and isoprene.

$$\text{SOA mass yield} = \frac{\Delta\text{SOA}}{\Delta\text{isoprene}} \times 100\% \quad (1)$$

Total nitrate contribution in HR-ToF-AMS measurements is derived primarily by the signal of the NO_2^+ and NO^+ ion. However, it is possible to distinguish the fractional contribution of organic nitrate to the total observed signal of nitrate. The organic nitrate fraction is determined using the ratio of the NO_2^+/NO^+ ions,[33] which is different for pure inorganic ammonium nitrate (typically between 0.3 to 0.5, e.g., Xu et al.[34]) than for pure organic nitrates (typically between 0.08 and 0.2). As the AMS instrument is calibrated with NH_4NO_3 particles, the ratio for the instrument for inorganic nitrate is known. The ratio for HR-ToF-AMS used in this study for inorganic nitrate is 0.41. Conservatively, the ratio to determine the fraction of organic nitrate is often chosen to be in the range of 0.1 (e.g., Kiendler-Scharr et al.[35]). However, recent studies[36] have shown that the organic nitrate ratio for isoprene nitrates can be much higher and can reach up to about 0.4, closer to the inorganic ratio. The exact values for the ratios of NO_2^+/NO^+ ions to distinguish between organic and inorganic nitrates vary between instruments and tuning of the instrument. While the ratio for inorganic nitrates is determined regularly during calibration of the AMS instrument, we additionally determined the organic nitrate ratio for isoprene and limonene nitrate SOA in the laboratory. While the results for the isoprene organic nitrates showed high ratios as seen in recent studies, the results were not sufficiently stable to unambiguously use the determined ratio. However, the limonene nitrate NO_2^+/NO^+ ion ratios could be determined to be 0.19. Although we did not do an extensive laboratory characterization of different organic nitrates from different BVOCs, the determined ratio for organic nitrate would also be comparable with the "ratio of ratios" approach.[37] Using the stable ratio for inorganic nitrate of 0.41 and the determined ratio for organic nitrate from lab experiments of 0.19, the ratio χ can be determined to be

$$\chi = \frac{R_{NH_4NO_3}}{R_{RONO_2}} \quad (2)$$

which is comparable to previously shown ratios.[37] Therefore, in the present study, we assume, for the isoprene organic nitrate ratio, at least a value of 0.19. We note that the ratio is likely higher for isoprene organic nitrates, so this reflects a lower limit. To explore the full range of possible organic nitrate formation in the SAPHIR chamber experiments, the range of organic nitrates was calculated by assuming ion ratios of 0.15 (a conservative lower estimate), 0.19, and 0.25, providing the range of the possible SOA yields for all experiments. The ratio of NO_2^+/NO^+ = 0.25 as an upper limit was chosen based on the assumption that all measured nitrate with AMS is explained by organic nitrate, that is, the total nitrate concentration measured equals the derived organic nitrate concentration. For all experiments except one, the ratio of 0.25 explains the upper limit of mass yields of organic nitrates, not accounting for possible heterogeneous reactions and formation and partitioning of HNO_3 into the aerosols. To determine total SOA mass yields, that is, yields for organic and organic nitrate partitioning to the aerosols, the organic nitrate yields determined for the ratio of 0.25 was used and added to the organic mass concentration to calculate an upper limit of total SOA mass yield for each experiment.

2.5. Gas-Particle Partitioning Coefficient Determination. For each seeded experiment, we can calculate an aggregate gas-particle partitioning coefficient for the total ANs. For this calculation, we again use the TD−CRDS measurements of total ANs, in combination with the measurements of aerosol-phase organic nitrate from the aerosol mass spectrometer described above and SMPS measurements of total aerosol volume, which is converted to mass loading. The AMS organic nitrate aerosol time series are reported in micrograms per cubic meter ($\mu g\ m^{-3}$); in order to make compatible with total AN concentrations in ppbv, these AMS measurements were converted to mixing ratios (ppbv) using the molecular

https://dx.doi.org/10.1021/acsearthspacechem.0c00311
ACS Earth Space Chem. 2021, 5, 785−800

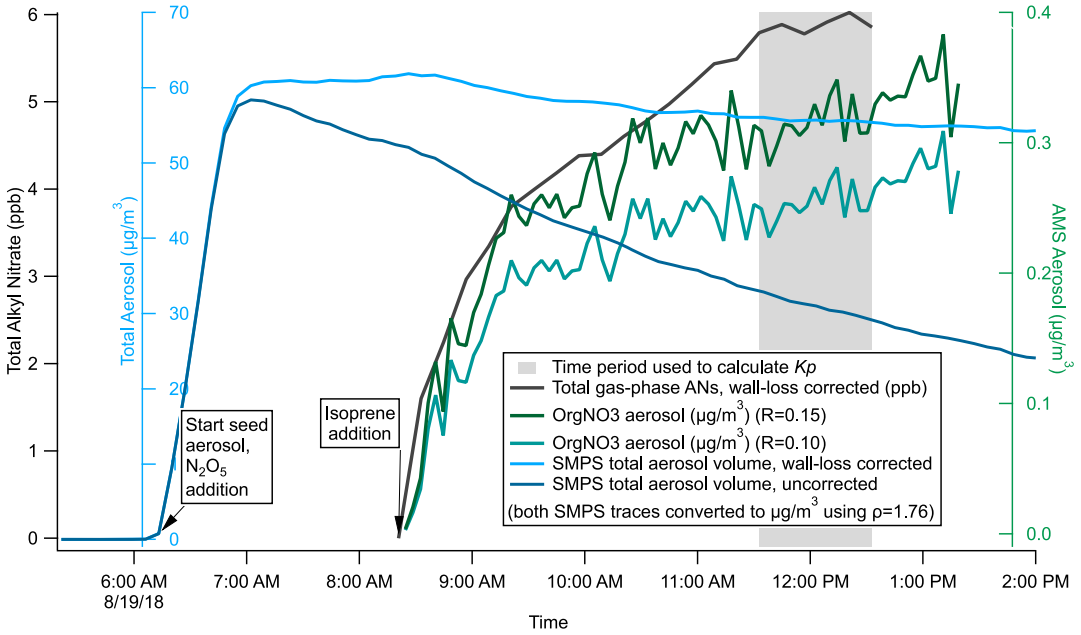

Figure 5. Data from 19 August 2018 experiment demonstrate how data was analyzed to calculate partitioning coefficients (K_p). This graph shows the AMS data for two different NO_2^+:NO^+ ratio assumptions. These two nitrate measurements were used to calculate the upper and lower limits for the K_p values (see Table 3).

weight of the nitrate fragment (62 g/mol). A measure of the total aerosol in the chamber throughout the experiments was obtained using a scanning mobility particle spectrometer (SMPS, TSI Classifier 3080 and TSI CPC 3787 low flow), which measured in the size range 0 to 431 nm-diameter particles. SMPS data were reported in cubic nanometers per cubic centimeters (nm^3 cm^{-3}) and were converted to micrograms per cubic meter by assuming a density of 1.76 g cm^{-3}, the measured density of ammonium sulfate,[38] which is the dominant component of the aerosol (>90%) for all experiments. The aggregate absorptive partitioning coefficient for each experiment was then calculated as

$$K_p = \frac{C_{aero}}{C_{gas} \times M_t} \quad (3)$$

This K_p equation is adapted from gas-particle partitioning coefficient equations.[39] A period of stability toward the end of each experiment was selected for the K_p determination (see Figure 5 for an example). The average TD−CRDS gas-phase AN signal during this period was used as the c_{gas}, the AMS OrgNO3 was used as the c_{aero}, and the SMPS mass loading (μg m^{-3}) was used as the M_t. We use the wall-loss-corrected data for c_{gas} and c_{aero} but use measured SMPS data without wall loss correction for M_t; this assumes that the semi-volatile AN species remain available for repartitioning from the walls but that aggregate gas/aerosol partitioning of these nitrates depends on the aerosol mass suspended in the chamber, not including seed aerosol that has deposited onto the chamber walls. Both wall-loss-corrected and uncorrected SMPS traces are shown in Figure 5 to enable evaluation of the potential effect of this assumption.

We note that because the SMPS size range (0−431 nm diameter) is smaller than the AMS size range (PM_1), all SMPS-based M_t measurements may be slightly low. The (small) magnitude of this effect can be seen in Figure 5, where the dilution and wall-loss corrected SMPS trace nevertheless decreases slightly (<10%) over the latter 5 h of the experiment. We do not attempt to correct for this, since as mentioned above, we assume that only the still-suspended measured aerosol mass should be included in M_t. Based on the observed decrease in the corrected SMPS trace, we expect that this would be a less than 10% effect.

3. RESULTS AND DISCUSSION

These experiments sought to explore product yields and gas-particle partitioning in NO_3 + isoprene reaction under different chemical regimes. Experiments were run with differing initial concentrations of isoprene, NO_2, and O_3 in an effort to explore regimes favoring different dominant RO_2 loss pathways from the initially produced isoprene nitrato-peroxy radicals. Recent computational modeling[46] based on this same chamber campaign has explored the fates of initially produced RO_2 in more detail. Using the latest structure−activity relationships for rate constants, this study found that the dominant nitrato-peroxy radical actually has a very slow reaction rate with other RO_2, so while some experiments did have larger RO_2 + RO_2 branching, this reaction was never dominant (see Table S3 for % RO_2 reaction via unimolecular loss, HO_2, NO_3, and RO_2, for four representative experiments). We therefore designate RO_2 regimes for the various experiments as "RO_2 + HO_2," "RO_2 enhanced," and "isomerization enhanced," the latter two of which, as shown in Table S3, actually feature a mix of RO_2 reaction paths. A major finding of this paper is that AN yields, SOA yields, and gas/aerosol partitioning of ANs all seem to be largely independent of the initial conditions explored (Table S1).

3.1. AN Yields and Comparison of Bulk to Speciated Nitrate Time Series. AN yields for all 15 experiments are listed in Table 1. Figure 6 shows the total wall-loss-corrected AN measurements for each experiment, plotted against the corresponding isoprene consumed (calculated as described above). As these data are both in ppb, the slope of these lines give the molar yield of ANs from the NO_3 + isoprene reaction.

https://dx.doi.org/10.1021/acsearthspacechem.0c00311
ACS Earth Space Chem. 2021, 5, 785−800

Table 1. AN Yields by Experiment Date[a]

Date	Reaction Pathway	Isoprene Consumed by NO_3 (ppbv)	Alkyl Nitrate Buildup (ppbv)	ANs Molar Yield (%)
3 Aug 2018	Test	2.3 ± 0.5	2.13 ± 0.1	86 ± 19
6	Test	3.96 ± 0.5	2.8 ± 0.1	90. ± 12
7	RO_2 isomerization enhanced, low RH	4.16 ± 0.5	1.9 ± 0.15	46 ± 7
8	RO_2 enhanced, dry	14.44 ± 1.4	11.1 ± 0.3	101 ± 10
9	*RO_2 + HO_2, dry*	*3.18 ± 0.5*	*3.3 ± 0.2*	*140 ± 24*
10	isom enhanced, dry	2.46 ± 0.5	1.75 ± 0.08	94 ± 20
12	*RO_2 enhanced, dry*	*4.81 ± 0.5*	*3.9 ± 0.2*	*112 ± 13*
13	RO_2 enhanced, dry	11.63 ± 1.2	10.5 ± 0.14	119 ± 12
14 Aug 2018	RO_2 enhanced, dry, AS seed	10.28 ± 1.0	9.23 ± 0.09	105 ± 11
15	RO_2 enhanced, humid, AS seed	10.22 ± 1.0	8.39 ± 0.09	106 ± 11
16	*isom enhanced, humid, AS seed*	*4.2 ± 0.5*	*2.7 ± 0.2*	*74 ± 10*
18	isom enhanced, humid, AS/org. coated seed	4 ± 0.5	2.1 ± 0.1	71 ± 9
19	RO_2 enhanced, no O_3, dry, AS seed	3.03 ± 0.5	6.04 ± 0.06	90. ± 15
20	RO_2 enhanced,humid, AS/org. coated seed	5.48 ± 0.6	3.55 ± 0.08	60. ± 6
21	*RO_2 + HO_2, humid*	*3.57 ± 0.5*	*4.3 ± 0.2*	*118 ± 17*

[a]White background rows are gas-phase experiments, and gray background rows are seeded. These AN yields were calculated as the slope of wall-loss-corrected total ANs vs calculated isoprene consumed by NO_3. See the text for discussion of the uncertainties on each variable. The four entries that are *italicized* indicate dates on which the TD−CRDS instrument NO_2 measurement showed poor correlation with the unified NO_2 data set produced by the MPI CRD instrument (see discussion around Figure 2).

The aggregate campaign data plotted here show that while there is some scatter among the individual experiments, the data taken all together suggest nominally 100% molar yield of ANs from the NO_3 + isoprene reaction (see the 1:1 line on the plot). There are no clear differences in these yield curves across seeded/unseeded experiments or across RH (Figure S3). Across RO_2 regimes (Figure S4), small differences do emerge. Within the RO_2 + RO_2 regime experiments, substantial scatter is observed, but the two RO_2 + HO_2 regime experiments appear to have higher yields, possibly due to contribution from NO_3 + propene ANs, and the isomerization experiments appear to have lower yields, potentially due to some loss of NO_2 from isomerization products.

A global fit to all data is shown in Figure 6, with the vertical portions of presumably later generation dinitrate formation removed (see the text below). The linear fit equation is $y = (1.08 \pm 0.02)x + (-0.34 \pm 0.09)$. Because these global fit slope uncertainties are smaller than our inferred 10% uncertainty in the AN concentration measurement and on the isoprene measurement (see Section 2.2), we apply as our relative error 14% (based on both the numerator and denominator having a 10% relative uncertainty) and conclude that the molar AN yield based on this global fit is 108 ± 15%. An alternative way to determine the overall AN yield is to average the yields determined from individual experiments, propagating their uncertainties. This approach, omitting the four italicized flagged as uncertain yield data points, gives an overall yield range of 90 ± 40% and, including all yield data points, gives 90 ± 50%.

This molar AN yield is larger than previous observations of 65−80%[9,40−45] but is consistent with aggregated chemical mechanisms of isoprene + NO_3 oxidation, for example, the master chemical mechanism (http://mcm.leeds.ac.uk/MCM/browse.htt?species=C5H8), in which none of the major NO_3 + isoprene products lose the initially added NO_3 group. A recent review[13] found that while most of the stable products from RO_2 + RO_2 or RO_2 + HO_2 contain a nitrate group, some RO_2 isomers preferentially form MVK + NO_2, which would reduce

https://dx.doi.org/10.1021/acsearthspacechem.0c00311
ACS Earth Space Chem. 2021, 5, 785−800

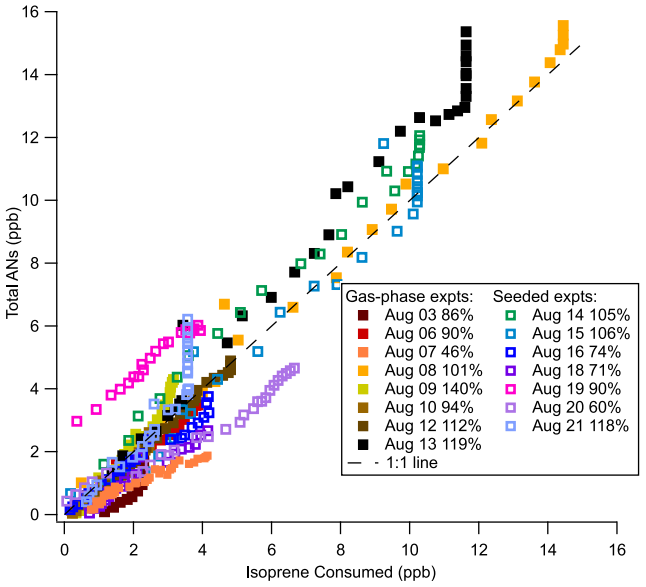

Figure 6. Wall-loss-corrected total ANs versus the isoprene consumed by NO_3. The dashed line is the 1:1 line. In aggregates, this shows that AN molar yields are similar across gas-phase and seeded experiments and are all close to 100% yield. A global fit of these data from all experiments has a slope corresponding to a molar yield of (108 ± 2)%, when the vertical portions are removed (these presumably represent dinitrate formation). Adding in the uncertainty of the ANs measurements and isoprene consumed, we determine a molar yield of (108 ± 15)%. An uncertainty-weighted average of the individual yields gives a molar yield of (90 ± 40)%. See the Supporting Information for versions of this plot split by RH and RO_2 regimes.

AN yields. Recent modeling and quantum chemical results[46] indicate that the published MVK formation is biased high. These experimental results also support the conclusion that in fact, very few of the originally formed nitrato-peroxy radicals decompose, losing the NO_2 moiety.

An AN yield of nominally 100% suggests that organonitrate hydrolysis is not rapid on the timescale of these experiments. Previous studies have found the hydrolysis lifetime of organic nitrates from NO_3 oxidation of monoterpenes to be on the order of hours under ambient conditions,[47] with the slower rate for NO_3 versus OH products arising because the NO_3-initiated oxidation reactions are likely to produce mostly primary and secondary organonitrate groups, while the tertiary nitrates are the fastest to hydrolyze.[48,49] A recent chamber study of NO_3 oxidation products of α- and β-pinene finds much more rapid hydrolysis (<30 min), albeit with only a small fraction of the organonitrate products hydrolyzable (9–17%).[50] To our knowledge, the hydrolysis rates of the nitrates formed from NO_3 + isoprene have not been measured, although Vasquez et al.[51] observed rapid hydrolysis of the tertiary nitrates formed by OH-initiated oxidation in the presence of NO.

For several experiments (08 August, 13 August, 14 August, 15 August, and 21 August), vertical portions of the plot are visible in Figure 6, suggesting that ANs continue to be produced after the isoprene was fully consumed. This is likely due to oxidation of the second double bond in isoprene, resulting in dinitrate formation. The oxidation of the two double bonds appears to proceed at significantly different enough rates that instead of observing an upward curvature in the yield curves, we see mostly linear correlations until the isoprene precursor is depleted, and only then does the second double bond begin to oxidize. However, we do observe some upward curvature later in the experiments which may be the reason for the >100% yield. We interpret this as meaning that averaged across all experiments, essentially all of the NO_3-reacted isoprene produces an AN product, and on the timescale of these experiments, some of those first-generation products will be further oxidized to dinitrates. We note that these experiments were not uniformly run for a consistent period of time after the isoprene was consumed, so we caution the interpretation of the presence or absence of this vertical portion of the yield curves as definitive.

Figure 7 shows two CIMS data sets compared to the total AN measurements from the 10 August 2018 dry, unseeded,

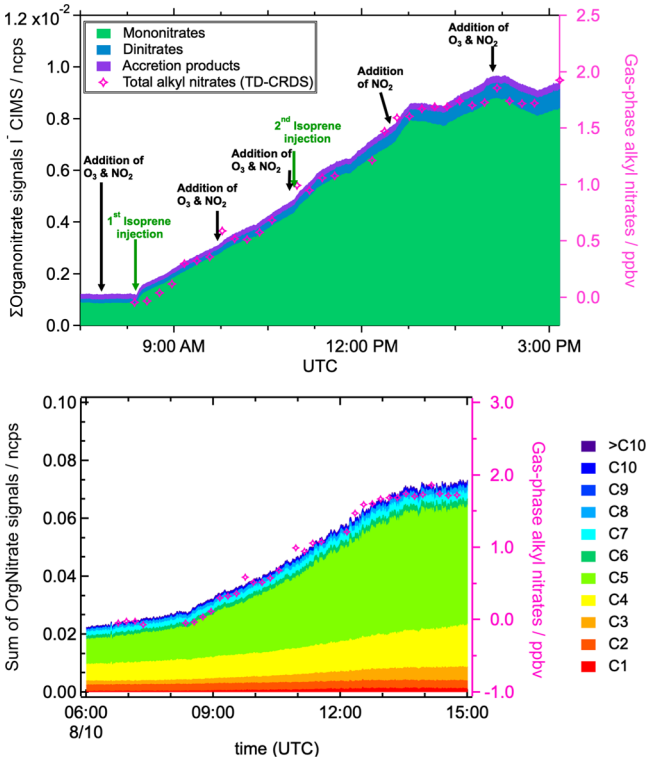

Figure 7. Upper panel: time series of classes of summed organonitrates measured by I^- CIMS (normalized counts per second), compared to total AN time series. Lower panel: time series of organic nitrate signals of various carbon numbers measured by Br^- CIMS (normalized counts per second), compared to total AN time series. All data are uncorrected for wall losses. These comparisons show some later formation of dinitrates that may be responsible for the larger than 100% AN yield.

and RO_2 isomerization regime experiment to investigate this interpretation. Although this is not a date for which the largest effect was observed in the AN yield curve, this is evidence of the ubiquity of some contribution of second-generation chemistry. Both I^- CIMS (upper) and Br^- CIMS (lower) summed signals show general agreement with the total AN time-series shape. Also, in both CIMS analyses, we observe an increase in dinitrates at later times and after additional NO_3 additions.

We note that the variable magnitude of the vertical (secondary) portion of the yield curves could arise not only from chemical variability but also from differing lengths of experiment; we observe it in some but not all RO_2-enhanced

https://dx.doi.org/10.1021/acsearthspacechem.0c00311
ACS Earth Space Chem. 2021, 5, 785–800

Table 2. SOA Yields for All Seeded Experiments[a]

date	reaction pathway	VOC reacted (ppb)	total SOA mass (μg m^{-3})	SOA yield (OA + $OrgNO_{3max}$) %	SOA yield (%) $OrgNO_3$ with different R (NO_2^+:NO^+):		
					R = 0.1	0.19	$OrgNO_3$ = max (0.15 to 0.27)
14 August 2018	RO_2 enhanced, dry,AS seed	12.1	5.4	15.2 ± 3.4	3.9 ± 0.9	5.8 ± 1.3[b]	5.8 ± 1.3
15 August 2018	RO_2 enhanced, humid, AS seed	12.5	5.0	13.3 ± 2.3	3.4 ± 0.3	5.2 ± 1.1	6.4 ± 1.5
16 August 2018	isom enhanced, humid, AS seed	5.8	2.2	12.9 ± 2.2	2.4 ± 0.5	3.5 ± 0.7	5.8 ± 1.1
19 August 2018	RO_2 enhanced no O_3, dry, AS seed	4.3	0.5	4.0 ± 0.8	2.5 ± 0.5	3.2 ± 0.6	3.2 ± 0.6
21 August 2018	RO_2 + HO_2, humid, AS seed	3.5	0.36[c]	3.5 ± 0.6[c]	1.7 ± 0.3	2.5 ± 0.4	3.5 ± 0.6

[a]In the OA + $OrgNO_3$ column, yields reported were determined as the ratio of the sum of OA and maximum $OrgNO_3$ to either (measured/modeled) Δisoprene. In the $OrgNO_3$ columns, the ΔSOA is determined based on the $OrgNO_3$ signal alone, with varying ratios as described in the text. The uncertainty is determined by assuming a 20% variation in the accuracy of the AMS mass concentration and a 10% error for the concentration of the consumed isoprene. [b]This yield uses R = 0.15, which is the maximum in this case. [c]Change in OA mass was not discernible, so these are based on maximum $OrgNO_3$ mass only.

and HO_2-enhanced experiments (see Figure S4). We also note that the amplitude of the vertical sections of the yield curves in Figure 6 is highly dependent on the wall loss correction factor used, since these losses compound and are the largest at the end of the experiments, and in many cases, the experimental conditions were changed (e.g., roof opened to initiate photooxidation) or terminated shortly after isoprene was consumed, omitting most secondary nitrate formation. Thus, we cannot quantify the AN yield of this second double-bond oxidation.

All yields are reported in Table 1, alongside reaction regime, isoprene consumed, and final AN buildup levels, to show differences between experiments. More details about each experiment can be found in Supporting Information, Table S1. Yields are determined as the slope of a linear fit to ANs versus isoprene consumed (see Figure 3). The uncertainty on each experiment's yield based on the slope error is typically below 5% because the fits are quite linear with little scatter. Thus, we make a more conservative estimate of the individual AN yield uncertainty, by propagating the uncertainties on the final AN buildup and final isoprene consumed at the end of each experiment (see Table 1) and applying this relative error to the AN yield from the individual experiment slopes. Uncertainties reported on AN buildup are based on the standard deviation of the AN measurements at the end of each experiment. Uncertainties in isoprene consumed are harder to determine, in large part because the OH concentration in most experiments was below the detection limit, leaving this variable contribution to isoprene loss rates unknown. The resulting estimated uncertainties in isoprene consumed are 10% relative uncertainty or 0.5 ppbv, whichever is larger. This is a maximum error which allows for OH concentrations at the limit of detection of the laser-induced fluorescence instrument. These relative errors are propagated in quadrature to obtain an estimate of each individual experiments' yield uncertainty. In the global fit to all yield data (Figure 6), we conclude that the slope error encompasses the scatter observed across experiments and thus represents a good estimate of the aggregate uncertainty.

Figure S5 shows several plots of AN yields as a function of various experimental parameters, to investigate whether any dependencies exist that explain the observed variability in individual experiment yields. We see generally more variability in the lower concentration experiments, lower isoprene consumed, lower final AN buildups, and more variability in higher-RH experiments, but no clear trends. This observation underpins our decision to collectively fit all yield data together to obtain the best estimate of AN yield and accompanying uncertainty.

3.2. SOA Yields. All SOA yields calculated for the seeded experiments are reported in Table 2 (SOA was only measurable for the seeded experiments). SOA yields for organic nitrates (ratio of ΔSOA = $\Delta OrgNO_{3part}$ to isoprene consumed by NO_3 radicals) were calculated (Eq 1) using different ratios for NO_2^+/NO^+ of 0.1, 0.19, and the maximum ratio (ranging from 0.15 to 0.27) for each experiment which explains all measured nitrate as organic nitrate ($OrgNO_3$ = max) and are shown in columns 6 to 8 in Table 2. These are shown to illustrate the variability due to the choice of the NO_2^+/NO^+ ratio; the boldface, gray background column 5 includes all organic + OrgNO3 aerosol mass (ratio of ΔSOA = ΔOA + $\Delta OrgNO_{3part,max}$ to isoprene consumed by NO_3 radicals) and is our recommended estimate for the SOA mass yield, representing isoprene nitrate partitioning to the aerosol phase (which consisted of typically ∼50 μg m^{-3} ammonium sulfate seed aerosol and ∼2−5 μg m^{-3} SOA). The total SOA mass yields range from 4.0 to 15.2% with most total SOA mass yields ranging between 13 to 15% (at a total SOA mass of ∼2−5 μg m^{-3}; the low mass yields of 4% correspond to total SOA mass <1 μg m^{-3}). Our results can be compared to and put into perspective with previous studies determining SOA yields from nitrate radical reactions with isoprene.[8,9]

In Ng et al.,[8] total SOA mass yields range between 4.3 and 23.8%, for VOC reacted from 18.4 to 101.6 ppb, and total SOA mass concentrations of 100−180 μg m^{-3} (significantly higher than this study). Ng et al. performed the experiments under dry conditions and varied the amount of the oxidation with regard to what is called "typical," "slow isoprene injection," and "slow N_2O_5 injection" in SOA yield experiments. The "slow N_2O_5 injection" reaction condition is targeted to enhance the RO_2 + RO_2 reaction, which should lead to a significantly higher production of condensable isoprene products. Our experiments in this study do not reproduce the same high yields for the RO_2-enhanced chemical regimes, perhaps because we never achieved sufficiently high RO_2 concentrations to truly favor RO_2 + RO_2 reactions (see Supporting

https://dx.doi.org/10.1021/acsearthspacechem.0c00311
ACS Earth Space Chem. 2021, 5, 785−800

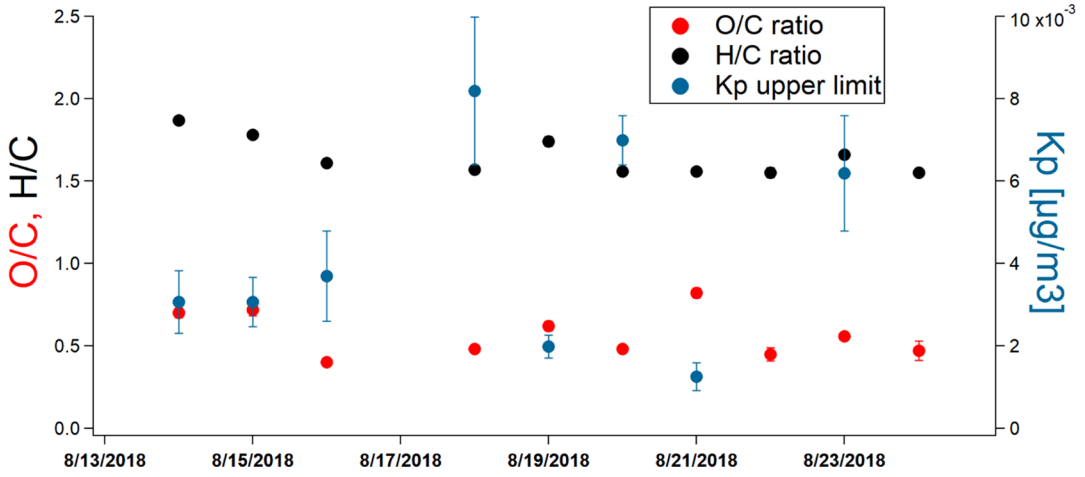

Figure 8. There are no major differences across seeded experiments in terms of bulk aerosol composition, as assessed by elemental ratios. Being plotted against the observed partitioning coefficients (K_p) demonstrates that SOA composition does not explain any of this variability.

Table 3. Experimentally Determined K_p Values ($K_p = \frac{C_{aero}}{C_{gas} \times M_t}$) for Seeded Experiments

date	Regime	K_p (m^3 μg^{-1}) "lower limit estimate" of $OrgNO_3$ assuming R = 0.10	K_p (m^3 μg^{-1}) $OrgNO_3$ "best estimate" assuming R = 0.19 or 0.15
14 August 2018	RO_2 enhanced	$1.6 \pm 0.4 \times 10^{-3}$	$2.4 \pm 0.6 \times 10^{-3}$
15 August 2018	RO_2 enhanced	$1.6 \pm 0.3 \times 10^{-3}$	$2.4 \pm 0.5 \times 10^{-3}$
16 August 2018	isom enhanced	$2.0 \pm 0.6 \times 10^{-3}$	$3.0 \pm 0.9 \times 10^{-3}$
18 August 2018	isom enhanced	$4.3 \pm 1.0 \times 10^{-3}$	$6.5 \pm 1.5 \times 10^{-3}$
19 August 2018[a]	RO_2 enhanced	$1.3 \pm 0.2 \times 10^{-3}$	$1.6 \pm 0.2 \times 10^{-3}$
20 August 2018[a]	RO_2 enhanced	$4.5 \pm 0.4 \times 10^{-3}$	$5.6 \pm 0.5 \times 10^{-3}$
21 August 2018	$RO_2 + HO_2$	$6.8 \pm 1.8 \times 10^{-4}$	$1.0 \pm 0.3 \times 10^{-3}$

[a]Noted experiments (19th and 20 August) were calculated using R = 0.15 as the maximum $OrgNO_3$ to determine c_{aero} instead of R = 0.19. All others used R = 0.19.

Information, Table S3). The major differences between the experiments is the large difference in isoprene precursor concentrations (18 to 203 ppbv in Ng et al.; 5 to 20 ppbv in this work) and the resulting differences in organic aerosol mass (5 to 70 μg m^{-3} in Ng et al.; 0.5 to 5 μg m^{-3} in this work).

The chamber SOA yields from Rollins et al.[9] are most comparable to our study since the experimental conditions are similar and performed in the same chamber. Rollins et al. determined an SOA mass yield of 2% where first-generation chemistry should be the dominant contributor and 14% ± 6% including secondary generation oxidation reactions. Therefore since, in this work, only the maximum SOA yield was calculated, it should be compared to the results including secondary chemistry, and the results agree within error margins (13 to 15% here vs 14% ± 6% in Rollins, et al.). The exceptions are the 19 August and 21 August experiments, both of which had substantially lower total organic aerosol mass (<0.5 μg m^{-3}) and lower SOA yields of ∼4%.

This work additionally extends the complexity and the chemical regimes tested with regard to SOA mass yield compared to both previous studies. As can be seen from Tables 2 and S1, with the exception of lower yields for the experiments with lower total organic aerosol loading, no clear trend or variability can be observed for the SOA mass yield. Yields seem to be mostly independent of the initial reaction pathways. This indicates that although different products of the isoprene oxidation are very likely formed due to the different initial conditions, there does not seem to be an effect on the overall amount of condensable material with regard to the amount of consumed precursor. This is similar to the observation for AN yields, where also no significant trend with regard to the different regimes could be observed.

Furthermore, no relationship is found between AN yields and SOA mass yields (Figure S6). Using the high-resolution information of AMS, the O:C ratio of the aerosol was determined for the same time period and the yields were calculated (Figure 8). Similar to what was observed for the SOA mass yields, the bulk chemical composition with regard to O:C ratios is not showing any observable trend with regard to different chemical regimes. Either the product distribution of the condensable species is very similar and does not affect the overall composition with regard to carbon and oxygen content or this method is not sensitive enough to detect potentially minor differences due to a different product spectrum in the aerosol.

We note that while broadly agreeing with previous chamber experiments, these chamber-measured SOA yields from NO_3 + isoprene are lower than the yields inferred from two recent field studies. In Fry et al.,[10] the NO_3 + isoprene SOA mass yield was estimated to be (27 ± 14)%, based on power plant plume intercepts during night flights in the 2013 SENEX campaign. In Zaveri et al.,[52] NO_3 + isoprene SOA mass yields are estimated to range from 0 to 55%, based on morning flights in the residual layer during the 2010 CARES campaign. These field-based estimates of NO_3 + isoprene SOA mass yield are of course subject to various assumptions about the fraction of OA that is due to this chemistry, model-based estimates of isoprene consumed, and so forth; however, the fact that these field

https://dx.doi.org/10.1021/acsearthspacechem.0c00311
ACS Earth Space Chem. 2021, 5, 785−800

Table 4. Theoretical K_p Values[a]

Number of Functional Groups						Product, MW (amu)	Theoretical K_p ($m^3\ \mu g^{-1}$)
C	NO_3	OH	C=O	OOH	R-O-O-R		
5	1	--	1	--		isoprene carbonyl nitrate, 145[a]	5.26×10^{-7}
5	1	1	--	--		isoprene hydroxy nitrate, 147[a]	9.85×10^{-6}
5	1	2	--	--		isoprene dihydroxy nitrate, 161[a]	1.47×10^{-3}
5	1	1	1	--		isoprene hydroxy carbonyl nitrate, 163[a]	7.68×10^{-5}
5	1	--	--	1		isoprene nitrato peroxide, 163[a]	1.60×10^{-5}
5	1	1	--	1		isoprene hydroxy nitrato peroxide, 179[a]	2.38×10^{-3}
5	1	2	1	--		179	1.14×10^{-2}
5	1	1	1	1		195	1.88×10^{-2}
5	2	2	--	--		isoprene dihydroxy dinitrate, 226[b]	1.71×10^{-1}
10	2	1	--	--	1	308	2.67×10^{-1}

[a]The highlighted red product is a monomer, the green is a dinitrate, and the blue is a dimer. The experimentally determined average volatility corresponds most closely to a trifunctional monomer (orange). Product names listed are from referenced papers. [b]Structures mechanistically predicted by Schwantes et al. (2015). [c]Structures mechanistically predicted by Rollins et al. (2009).

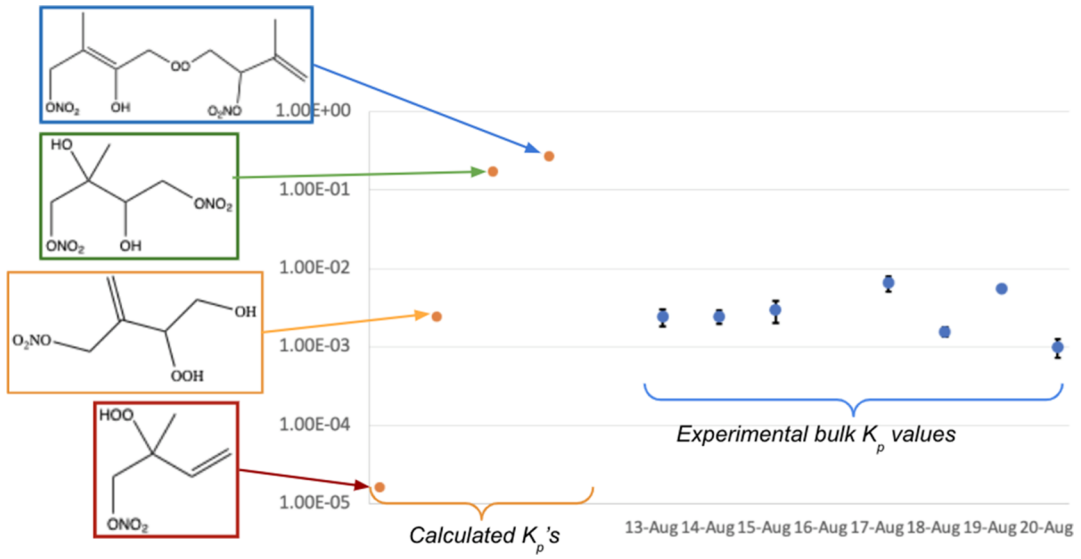

Figure 9. Group contribution calculated partitioning coefficients (left, color-coded to Table 4) for four potential representative isoprene + NO_3 product structures, compared to the experimentally measured bulk K_p values from the currently reported set of seeded experiments. The empirical K_p values were calculated using $OrgNO_3$ for an NO_2^+:NO^+ ratio of 0.19.

yields were substantially higher suggests that chamber experiments might have not yet explored the chemical regime responsible for ambient SOA production from NO_3 + isoprene.

3.3. Gas-Particle Partitioning of ANs. To obtain a range of possible bulk K_p values to describe the gas-aerosol partitioning of total ANs, two different aerosol organic nitrate data sets from AMS were used, in conjunction with total ANs measured by TD−CRDS and total aerosol mass determined via SMPS. The two AMS data sets were different fractions of the full measurement defined by different ratios of how much product was in the particle phase: the upper limit and the "best estimate" of K_p values was determined using the $OrgNO_3$ signal using R = 0.19 to partition the organic nitrate and the lower limit estimate of K_p was calculated using the $OrgNO_3$ determined with R = 0.10, both using the method described above in Section 2.5. The resulting experimental K_p values are reported in Table 3.

In order to interpret the empirically observed bulk K_p's, theoretical K_p values were calculated using predicted vapor pressure p_L^0 from a simplified group contribution method (SIMPOL.1, Pankow and Asher[53]). The SIMPOL group contribution predicts the vapor pressure based on the number and type of the functional group on a molecule, and vapor pressures were then converted to K_p using eq 4, as described in Pankow.[39] A few possible likely structures and the corresponding calculated K_p values can be found in Table 4 below.

$$K_{p,\text{theoretical}} = \frac{760RTf_{om}}{MW10^6\varsigma p_L^0} \quad (4)$$

https://dx.doi.org/10.1021/acsearthspacechem.0c00311
ACS Earth Space Chem. 2021, 5, 785−800

In the Pankow equation, K_p is the partitioning coefficient, f_{om} is the weight fraction that is the organic material phase and is assumed to be 1, T is the temperature, 295 K, MW_{om} is the molecular weight, in g/mol, of the organic compound, ζ is the activity coefficient and also assumed to be 1, and p_L^0 is the vapor pressure in atm, which was predicted using the group contribution method. The smaller theoretical K_p values indicate higher volatility and less product in the aerosol phase. Another forthcoming NO_3Isop paper (Wu et al.[54]) investigates the volatility of individual organonitrate compounds, finding a broad range of volatilities that span the range observed here but also include a small fraction (<2%) of much lower volatility, highly oxidized dimers.

The average aggregate experimental K_p value ($\sim 10^{-3}$ m^3 μg^{-1}) is closest to the value of the theoretical K_p of a trifunctional monomer structure, suggesting that most of the AN products are C_5 species. Figure 9 visualizes the experimental aggregate partitioning coefficient values, compared to the group contribution-calculated theoretical K_p values from different structures. We note that while this "average" AN product represents the majority of the products formed from the NO_3 + isoprene reaction, it is likely that less abundant, but substantially lower-volatility, products contribute disproportionately to the species partitioning to the particle phase. Because of how we calculate this aggregate partitioning coefficient, it represents all of the AN products, the majority of which do not contribute to SOA.

The I^- CIMS measurements of individual nitrates (example spectra are shown from 8 August and 10 August experiments in Figure 10) indicate that mononitrates are the dominant products, with dinitrates and dimers also observed. Compared to theoretical partitioning coefficients (Table 4) for the major observed mononitrate ($C_5H_9NO_5$: 1.60 × 10^{-5} m^3 μg^{-1}), dinitrate ($C_5H_6N_2O_8$: 1.71 × 10^{-1} m^3 μg^{-1}), and dimer ($C_{10}H_{16}N_2O_9$: 2.67 × 10^{-1} m^3 μg^{-1}), we see that the empirically observed bulk K_p's (Table 3, Figure 9) falling in the 10^{-3} m^3 μg^{-1} range suggest a substantially more volatile mix of organonitrates than the CIMS data, possibly indicating differential sensitivities to the classes of nitrates, or partitioning that is not driven by absorptive partitioning.

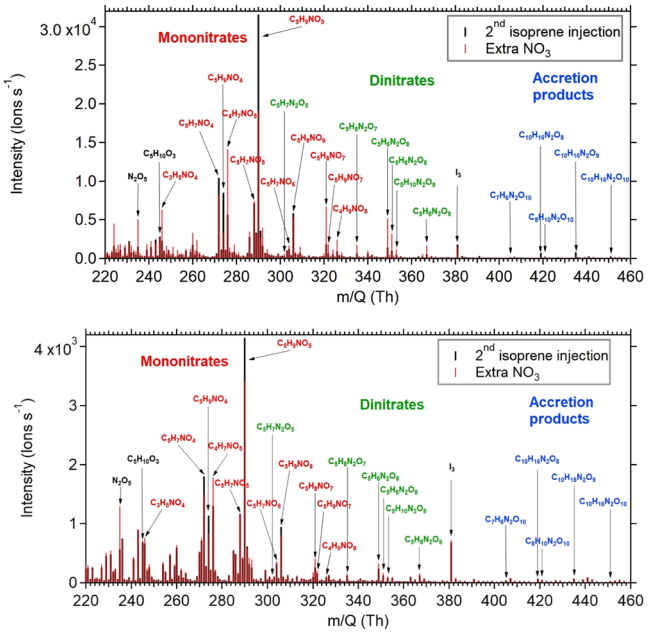

Figure 10. Representative I-CIMS data from 8 August (upper) and 10 August (lower) experiments. Gas-phase fragments detected include many nitrates.

Another report of volatility of SOA from NO_3 and isoprene is used in Pye et al.[47] based on Rollins et al.[9] The reported partitioning coefficient for the dinitrates assumed to be responsible for SOA formation in that study is K_p = 0.112 m^3 μg^{-1} (the inverse of the reported saturation concentration of C^* = 8.9 μg m^{-3}). This partitioning coefficient, because it represents a dinitrate, is significantly larger than the bulk partitioning coefficients calculated for these experiments. If this larger partitioning coefficient is assumed for the aggregate isoprene nitrate products, it would suggest that more products would partition into the particle phase than observed in these experiments.

4. CONCLUSIONS

A series of experiments at the SAPHIR chamber examined the oxidation of isoprene by NO_3. AN molar yield from NO_3 + isoprene is found to be (108 ± 15) %, SOA mass yields for the OA + $OrgNO_3$ mass are found to be 13 to 15%, and aggregated AN partitioning coefficients are consistent with average volatility corresponding to a trifunctional C_5 nitrate. The experiments described here were conducted under approximately ambient conditions of precursor concentrations and seed aerosol and provide a significant additional body of evidence for the substantial SOA yields from the NO_3 + isoprene reaction.

Overall, we conclude that AN yield is nominally 100% and that the organic nitrate partitioning coefficient, bulk aerosol composition, and SOA yields are largely independent of the chemical regime. Two exceptions are an observed slightly higher AN yield (120 to 140%, 2 experiments) in the HO_2 regime, potentially due to interfering propene nitrate, and slightly lower yield in the RO_2 isomerization regime (46 to 94%, 4 experiments), potentially due to some loss of the NO_2 group.

SOA mass yields are observed to be 13 to 15%, which is in general agreement with other chamber experiments conducted in similar regimes to those used in this study. Despite a significant variation in initial night-time oxidation conditions, the tested regimes cannot explain or identify unique conditions which could be responsible for the significantly higher SOA mass yields inferred for NO_3 + isoprene in aircraft measurements.[10,52]

■ ASSOCIATED CONTENT

Supporting Information

The Supporting Information is available free of charge at https://pubs.acs.org/doi/10.1021/acsearthspacechem.0c00311.

Experimental parameters; key instruments used for the alkyl nitrate and aerosol analysis; breakdown of the reactive fate of the initially formed nitrate peroxy radicals; scatterplot NO_2 comparisons; thermogram on a chamber mix of isoprene + NO_3 products; total alkyl nitrate yield plots; AN yields plotted against several experimental variables; and SOA mass yield measurements (PDF)

https://dx.doi.org/10.1021/acsearthspacechem.0c00311
ACS Earth Space Chem. 2021, 5, 785−800

AUTHOR INFORMATION

Corresponding Author

Juliane L. Fry − *Chemistry Department and Environmental Studies Program, Reed College, Portland, Oregon 97202, United States;* orcid.org/0000-0003-1799-5828; Email: fry@reed.edu

Authors

Bellamy Brownwood − *Chemistry Department and Environmental Studies Program, Reed College, Portland, Oregon 97202, United States*

Avtandil Turdziladze − *Institute for Energy and Climate (IEK-8), Forschungszentrum Jülich, Jülich 52428, Germany*

Thorsten Hohaus − *Institute for Energy and Climate (IEK-8), Forschungszentrum Jülich, Jülich 52428, Germany*

Rongrong Wu − *Institute for Energy and Climate (IEK-8), Forschungszentrum Jülich, Jülich 52428, Germany*

Thomas F. Mentel − *Institute for Energy and Climate (IEK-8), Forschungszentrum Jülich, Jülich 52428, Germany*

Philip T. M. Carlsson − *Institute for Energy and Climate (IEK-8), Forschungszentrum Jülich, Jülich 52428, Germany;* orcid.org/0000-0002-5365-1689

Epameinondas Tsiligiannis − *Department of Chemistry and Molecular Biology, University of Gothenburg, Gothenburg 405 30, Sweden*

Mattias Hallquist − *Department of Chemistry and Molecular Biology, University of Gothenburg, Gothenburg 405 30, Sweden;* orcid.org/0000-0001-5691-1231

Stefanie Andres − *Institute for Energy and Climate (IEK-8), Forschungszentrum Jülich, Jülich 52428, Germany*

Luisa Hantschke − *Institute for Energy and Climate (IEK-8), Forschungszentrum Jülich, Jülich 52428, Germany*

David Reimer − *Institute for Energy and Climate (IEK-8), Forschungszentrum Jülich, Jülich 52428, Germany*

Franz Rohrer − *Institute for Energy and Climate (IEK-8), Forschungszentrum Jülich, Jülich 52428, Germany*

Ralf Tillmann − *Institute for Energy and Climate (IEK-8), Forschungszentrum Jülich, Jülich 52428, Germany*

Benjamin Winter − *Institute for Energy and Climate (IEK-8), Forschungszentrum Jülich, Jülich 52428, Germany*

Jonathan Liebmann − *Atmospheric Chemistry Department, Max Planck Institute for Chemistry, Mainz 55128, Germany*

Steven S. Brown − *Chemical Sciences Division, Earth System Research Laboratory, NOAA, Boulder, Colorado 80305, United States*

Astrid Kiendler-Scharr − *Institute for Energy and Climate (IEK-8), Forschungszentrum Jülich, Jülich 52428, Germany*

Anna Novelli − *Institute for Energy and Climate (IEK-8), Forschungszentrum Jülich, Jülich 52428, Germany*

Hendrik Fuchs − *Institute for Energy and Climate (IEK-8), Forschungszentrum Jülich, Jülich 52428, Germany;* orcid.org/0000-0003-1263-0061

Complete contact information is available at: https://pubs.acs.org/10.1021/acsearthspacechem.0c00311

Notes

The authors declare no competing financial interest.

ACKNOWLEDGMENTS

This project has received funding from the European Research Council (ERC) under the European Union's Horizon 2020 research and innovation programme (SARLEP grant agreement no. 681529) and from the European Commission (EC) under the European Union's Horizon 2020 research and innovation programme (Eurochamp 2020 grant agreement no. 730997). The authors thank the Forschungszentrum Jülich for travel support under the project "Seed Money". BB acknowledges the Reed College Opportunity Grant program for travel funding; JLF acknowledges the Fulbright U.S. Scholar Program (Netherlands) for enabling the origination and planning of this campaign. The CIMS analysis was supported by the Swedish Research Council (grant numbers 2014-05332 and 2018-04430) and Formas (grant number 942-2015-1537). We acknowledge valuable discussion with John Crowley, Patrick Dewald, Justin Shenolikdar, and Niels Friedrich.

REFERENCES

(1) Guenther, A. B.; Jiang, X.; Heald, C. L.; Sakulyanontvittaya, T.; Duhl, T.; Emmons, L. K.; Wang, X. The Model of Emissions of Gases and Aerosols from Nature Version 2.1 (MEGAN2.1): An Extended and Updated Framework for Modeling Biogenic Emissions. *Geosci. Model Dev.* **2012**, *5*, 1471−1492.

(2) Monson, R. K.; Jones, R. T.; Rosenstiel, T. N.; Schnitzler, J.-P. Why Only Some Plants Emit Isoprene. *Plant, Cell Environ.* **2013**, *36*, 503−516.

(3) Starn, T. K.; Shepson, P. B.; Bertman, S. B.; Riemer, D. D.; Zika, R. G.; Olszyna, K. Nighttime Isoprene Chemistry at an Urban-Impacted Forest Site. *J. Geophys. Res.: Atmos.* **1998**, *103*, 22437−22447.

(4) Beaver, M. R.; Clair, J. M. S.; Paulot, F.; Spencer, K. M.; Crounse, J. D.; LaFranchi, B. W.; Min, K. E.; Pusede, S. E.; Wooldridge, P. J.; Schade, G. W.; Park, C.; Cohen, R. C.; Wennberg, P. O. Importance of Biogenic Precursors to the Budget of Organic Nitrates: Observations of Multifunctional Organic Nitrates by CIMS and TD-LIF during BEARPEX 2009. *Atmos. Chem. Phys.* **2012**, *12*, 5773−5785.

(5) Sander, S. P.; Friedl, R. R.; Ravishankara, A. R. *Chemical Kinetics and Photochemical Data for Use in Atmospheric Studies Evaluation Number 14*; JPL Publication, 2011.

(6) Calvert, J. G.; Atkinson, R.; Becker, K. H.; Kamens, R. M.; Seinfeld, J. H.; Wallington, T. H.; Yarwood, G. *The Mechanisms of Atmospheric Oxidation of the Aromatic Hydrocarbons*; Oxford University Press, 2002.

(7) Brown, S. S.; Osthoff, H. D.; Stark, H.; Dubé, W. P.; Ryerson, T. B.; Warneke, C.; de Gouw, J. A.; Parrish, D. D.; Fehsenfeld, F. C.; Ravishankara, A. R. Aircraft Observations of Daytime NO_3 and N_2O_5 and Their Implications for Tropospheric Chemistry. *J. Photochem. Photobiol., A* **2005**, *176*, 270−278.

(8) Ng, N. L.; Kwan, A. J.; Surratt, J. D.; Chan, A. W. H.; Chhabra, P. S.; Sorooshian, A.; Pye, H. O. T.; Crounse, J. D.; Wennberg, P. O.; Flagan, R. C.; Seinfeld, J. H. Secondary Organic Aerosol (SOA) Formation from Reaction of Isoprene with Nitrate Radicals (NO_3). *Atmos. Chem. Phys.* **2008**, *8*, 4117−4140.

(9) Rollins, A. W.; Kiendler-Scharr, A.; Fry, J. L.; Brauers, T.; Brown, S. S.; Mensah, A.; Mentel, T. F.; Rohrer, F.; Tillmann, R.; Wegener, R.; Wooldridge, P. J.; Cohen, R. C. Isoprene Oxidation by Nitrate Radical: Alkyl Nitrate and Secondary Organic Aerosol Yields. *Atmos. Chem. Phys.* **2009**, *9*, 6685−6703.

(10) Fry, J. L.; Brown, S. S.; Middlebrook, A. M.; Edwards, P. M.; Campuzano-Jost, P.; Day, D. A.; Jimenez, J. L.; Allen, H. M.; Ryerson, T. B.; Pollack, I.; Graus, M.; Warneke, C.; de Gouw, J. A.; Gilman, J.; Lerner, B. M.; Dubé, W. P.; Liao, J.; Welti, A.; Welti, A. Secondary Organic Aerosol (SOA) Yields from NO_3 Radical + Isoprene Based on Nighttime Aircraft Power Plant Plume Transects. *Atmos. Chem. Phys.* **2018**, *18*, 11663−11682.

(11) Hoyle, C. R.; Berntsen, T.; Myhre, G.; Isaksen, I. S. A. Secondary Organic Aerosol in the Global Aerosol - Chemical Transport Model Oslo CTM2. *Atmos. Chem. Phys.* **2007**, *7*, 5675−5694.

(12) Schwantes, R. H.; Teng, A. P.; Nguyen, T. B.; Coggon, M. M.; Crounse, J. D.; St Clair, J. M.; Schilling, K. A.; Seinfeld, J. H.; Wennberg, P. O. Isoprene NO_3 Oxidation Products from the RO_2 + HO_2 Pathway. *J. Phys. Chem. A* **2015**, *119*, 10158−10171.
(13) Wennberg, P. O.; Bates, K. H.; Crounse, J. D.; Dodson, L. G.; McVay, R. C.; Mertens, L. A.; Nguyen, T. B.; Praske, E.; Schwantes, R. H.; Smarte, M. D.; St Clair, J. M.; Teng, A. P.; Zhang, X.; Seinfeld, J. H. Gas-Phase Reactions of Isoprene and Its Major Oxidation Products. *Chem. Rev.* **2018**, *118*, 3337−3390.
(14) Carlton, A. G.; Wiedinmyer, C.; Kroll, J. H. A Review of Secondary Organic Aerosol (SOA) Formation from Isoprene. *Atmos. Chem. Phys.* **2009**, *9*, 4987−5005.
(15) Chung, S. H.; Seinfeld, J. H. Global Distribution and Climate Forcing of Carbonaceous Aerosols. *J. Geophys. Res.* **2002**, *107*, 4407.
(16) Myhre, G.; Shindell, D.; Bréon, F.-M.; Collins, W.; Fuglestvedt, J.; Huang, J.; Koch, D.; Lamarque, J.-F.; Lee, D.; Mendoza, B.; Nakajima, T.; Robock, A.; Stephens, G.; Zhang, H.; Aamaas, B.; Boucher, O.; Dalsøren, S. B.; Daniel, J. S.; Forster, P.; Granier, C.; Haigh, J.; Hodnebrog, Ø.; Kaplan, J. O.; Marston, G.; Nielsen, C. J.; O'Neill, B. C.; Peters, G. P.; Pongratz, J.; Ramaswamy, V.; Roth, R.; Rotstayn, L.; Smith, S. J.; Stevenson, D.; Vernier, J.-P.; Wild, O.; Young, P.; Jacob, D.; Ravishankara, A. R.; Shine, K. Anthropogenic and Natural Radiative Forcing. *Climate Change 2013: The Physical Science Basis. Contribution of Working Group I to the Fifth Assessment Report of the Intergovernmental Panel on Climate Change*; Cambridge University Press, 2013; pp 659−740.
(17) Pope, C. A.; Dockery, D. W. Health effects of fine particulate air pollution: lines that connect. *J. Air Waste Manag. Assoc.* **2006**, *56*, 709−742.
(18) Lelieveld, J.; Evans, J. S.; Fnais, M.; Giannadaki, D.; Pozzer, A. The Contribution of Outdoor Air Pollution Sources to Premature Mortality on a Global Scale. *Nature* **2015**, *525*, 367−371.
(19) Hallquist, M.; Wenger, J. C.; Baltensperger, U.; Rudich, Y.; Simpson, D.; Claeys, M.; Dommen, J.; Donahue, N. M.; George, C.; Goldstein, A. H.; Hamilton, J. F.; Herrmann, H.; Hoffmann, T.; Iinuma, Y.; Jang, M.; Jenkin, M. E.; Jimenez, J. L.; Kiendler-Scharr, A.; Maenhaut, W.; McFiggans, G.; Mentel, T. F.; Monod, A.; Prevot, A. S. H.; Seinfeld, J. H.; Surratt, J. D.; Szmigielski, R.; Wildt, J. The Formation, Properties and Impact of Secondary Organic Aerosol: Current and Emerging Issues. *Atmos. Chem. Phys.* **2009**, *9*, 5155−5236.
(20) Marais, E. A.; Jacob, D. J.; Jimenez, J. L.; Campuzano-Jost, P.; Day, D. A.; Hu, W.; Krechmer, J.; Zhu, L.; Kim, P. S.; Miller, C. C.; Fisher, J. A.; Travis, K.; Yu, K.; Hanisco, T. F.; Wolfe, G. M.; Arkinson, H. L.; Pye, H. O. T.; Froyd, K. D.; Liao, J.; McNeill, V. F. Aqueous-Phase Mechanism for Secondary Organic Aerosol Formation from Isoprene: Application to the Southeast United States and Co-Benefit of SO_2 Emission Controls. *Atmos. Chem. Phys.* **2016**, *16*, 1603−1618.
(21) Kroll, J. H.; Ng, N. L.; Murphy, S. M.; Flagan, R. C.; Seinfeld, J. H. Secondary Organic Aerosol Formation from Isoprene Photooxidation. *Environ. Sci. Technol.* **2006**, *40*, 1869−1877.
(22) Liu, J.; D'Ambro, E. L.; Lee, B. H.; Lopez-Hilfiker, F. D.; Zaveri, R. A.; Rivera-Rios, J. C.; Keutsch, F. N.; Iyer, S.; Kurten, T.; Zhang, Z.; Gold, A.; Surratt, J. D.; Shilling, J. E.; Thornton, J. A. Efficient Isoprene Secondary Organic Aerosol Formation from a Non-IEPOX Pathway. *Environ. Sci. Technol.* **2016**, *50*, 9872−9880.
(23) Surratt, J. D.; Lewandowski, M.; Offenberg, J. H.; Jaoui, M.; Kleindienst, T. E.; Edney, E. O.; Seinfeld, J. H. Effect of Acidity on Secondary Organic Aerosol Formation from Isoprene. *Environ. Sci. Technol.* **2007**, *41*, 5363−5369.
(24) Fuchs, H.; Simpson, W. R.; Apodaca, R. L.; Brauers, T.; Cohen, R. C.; Crowley, J. N.; Dorn, H.-P.; Dubé, W. P.; Fry, J. L.; Häseler, R.; Kajii, Y.; Kiendler-Scharr, A.; Labazan, I.; Matsumoto, J.; Mentel, T. F.; Nakashima, Y.; Rohrer, F.; Rollins, A. W.; Schuster, G.; Tillmann, R.; Wahner, A.; Wooldridge, P. J.; Brown, S. S. Comparison of N_2O_5 Mixing Ratios during NO3Comp 2007 in SAPHIR. *Atmos. Meas. Tech.* **2012**, *5*, 2763−2777.
(25) Fuchs, H.; Novelli, A.; Rolletter, M.; Hofzumahaus, A.; Pfannerstill, E. Y.; Kessel, S.; Edtbauer, A.; Williams, J.; Michoud, V.; Dusanter, S.; Locoge, N.; Zannoni, N.; Gros, V.; Truong, F.; Sarda-Esteve, R.; Cryer, D. R.; Brumby, C. A.; Whalley, L. K.; Stone, D.; Seakins, P. W.; Heard, D. E.; Schoemaecker, C.; Blocquet, M.; Coudert, S.; Batut, S.; Fittschen, C.; Thames, A. B.; Brune, W. H.; Ernest, C.; Harder, H.; Muller, J. B. A.; Elste, T.; Kubistin, D.; Andres, S.; Bohn, B.; Hohaus, T.; Holland, F.; Li, X.; Rohrer, F.; Kiendler-Scharr, A.; Tillmann, R.; Wegener, R.; Yu, Z.; Zou, Q.; Wahner, A. Comparison of OH Reactivity Measurements in the Atmospheric Simulation Chamber SAPHIR. *Atmos. Meas. Tech.* **2017**, *10*, 4023−4053.
(26) Dewald, P.; Liebmann, J. M.; Friedrich, N.; Shenolikar, J.; Schuladen, J.; Rohrer, F.; Reimer, D.; Tillmann, R.; Novelli, A.; Cho, C.; Xu, K.; Holzinger, R.; Bernard, F.; Zhou, L.; Mellouki, W.; Brown, S. S.; Fuchs, H.; Lelieveld, J.; Crowley, J. N. Evolution of NO_3 Reactivity during the Oxidation of Isoprene. *Atmos. Chem. Phys.* **2020**, *1−29*, 10459−10475.
(27) Keehan, N. I.; Brownwood, B.; Marsavin, A.; Day, D. A.; Fry, J. L. Thermal Dissociation Cavity Ring-down Spectrometer (TD-CRDS) for Detection of Organic Nitrates in Gas and Particle Phase. *Atmos. Meas. Tech.* **2020**, *13*, 6255−6269.
(28) Sobanski, N.; Schuladen, J.; Schuster, G.; Lelieveld, J.; Crowley, J. N. A Five-Channel Cavity Ring-down Spectrometer for the Detection of NO_2, NO_3, N_2O_{55}, Total Peroxy Nitrates and Total Alkyl Nitrates. *Atmos. Meas. Tech.* **2016**, *9*, 5103−5118.
(29) IUPAC. Task Group on Atmospheric Chemical Kinetic Data Evaluation. http://iupac.pole-ether.fr/ (accessed April 22, 2020).
(30) Canagaratna, M. R.; Jayne, J. T.; Jimenez, J. L.; Allan, J. D.; Alfarra, M. R.; Zhang, Q.; Onasch, T. B.; Drewnick, F.; Coe, H.; Middlebrook, A.; Delia, A.; Williams, L. R.; Trimborn, A. M.; Northway, M. J.; DeCarlo, P. F.; Kolb, C. E.; Davidovits, P.; Worsnop, D. R. Chemical and Microphysical Characterization of Ambient Aerosols with the Aerodyne Aerosol Mass Spectrometer. *Mass Spectrom. Rev.* **2007**, *26*, 185−222.
(31) DeCarlo, P. F.; Kimmel, J. R.; Trimborn, A.; Northway, M. J.; Jayne, J. T.; Aiken, A. C.; Gonin, M.; Fuhrer, K.; Horvath, T.; Docherty, K. S.; Worsnop, D. R.; Jimenez, J. L. Field-Deployable, High-Resolution, Time-of-Flight Aerosol Mass Spectrometer. *Anal. Chem.* **2006**, *78*, 8281−8289.
(32) Jimenez, J. L.; Jayne, J. T.; Shi, Q.; Kolb, C. E.; Worsnop, D. R.; Yourshaw, I.; Seinfeld, J. H.; Flagan, R. C.; Zhang, X.; Smith, K. A.; Morris, J. W.; Davidovits, P.. Ambient Aerosol Sampling Using the Aerodyne Aerosol Mass Spectrometer. *J. Geophys. Res.: Atmos.* **2003**, *108* (). DOI: 10.1029/2001JD001213.
(33) Farmer, D. K.; Matsunaga, A.; Docherty, K. S.; Surratt, J. D.; Seinfeld, J. H.; Ziemann, P. J.; Jimenez, J. L. Response of an Aerosol Mass Spectrometer to Organonitrates and Organosulfates and Implications for Atmospheric Chemistry. *Proc. Natl. Acad. Sci. U.S.A.* **2010**, *107*, 6670−6675.
(34) Xu, L.; Suresh, S.; Guo, H.; Weber, R. J.; Ng, N. L. Aerosol Characterization over the Southeastern United States Using High Resolution Aerosol Mass Spectrometry: Spatial and Seasonal Variation of Aerosol Composition, Sources, and Organic Nitrates. *Atmos. Chem. Phys.* **2015**, *15*, 10479−10552.
(35) Kiendler-Scharr, A.; Mensah, A. A.; Friese, E.; Topping, D.; Nemitz, E.; Prevot, A. S. H.; Äijälä, M.; Allan, J.; Canonaco, F.; Canagaratna, M.; Carbone, S.; Crippa, M.; Dall Osto, M.; Day, D. A.; De Carlo, P.; Di Marco, C. F.; Elbern, H.; Eriksson, A.; Freney, E.; Hao, L.; Herrmann, H.; Hildebrandt, L.; Hillamo, R.; Jimenez, J. L.; Laaksonen, A.; McFiggans, G.; Mohr, C.; O'Dowd, C.; Otjes, R.; Ovadnevaite, J.; Pandis, S. N.; Poulain, L.; Schlag, P.; Sellegri, K.; Swietlicki, E.; Tiitta, P.; Vermeulen, A.; Wahner, A.; Worsnop, D.; Wu, H.-C. Ubiquity of Organic Nitrates from Nighttime Chemistry in the European Submicron Aerosol: Organic Nitrates in European PM1. *Geophys. Res. Lett.* **2016**, *43*, 7735−7744.
(36) He, Q.; Tomaz, S.; Li, C.; Zhu, D.; Meidan, D.; Riva, M.; Laskin, A.; Brown, S. S.; George, C.; Wang, X.; Rudich, Y. Optical Properties of Secondary Organic Aerosol Produced by Nitrate Radical

Oxidation of Biogenic Volatile Organic Compounds. *Environ. Sci. Technol.* **2021**, *55* (5), 2878−2889.
(37) Fry, J. L.; Draper, D. C.; Zarzana, K. J.; Campuzano-Jost, P.; Day, D. A.; Jimenez, J. L.; Brown, S. S.; Cohen, R. C.; Kaser, L.; Hansel, A.; Cappellin, L.; Karl, T.; Hodzic Roux, A.; Turnipseed, A.; Cantrell, C.; Lefer, B. L.; Grossberg, N. Observations of Gas- and Aerosol-Phase Organic Nitrates at BEACHON-RoMBAS 2011. *Atmos. Chem. Phys.* **2013**, *13*, 8585−8605.
(38) Sarangi, B.; Aggarwal, S. G.; Sinha, D.; Gupta, P. K. Aerosol effective density measurement using scanning mobility particle sizer and quartz crystal microbalance with the estimation of involved uncertainty. *Atmos. Meas. Tech.* **2016**, *9*, 859−875.
(39) Pankow, J. F. An Absorption Model of the Gas/Aerosol Partitioning Involved in the Formation of Secondary Organic Aerosol. *Atmos. Environ.* **1994**, *28*, 189−193.
(40) Barnes, I.; Bastian, V.; Becker, K. H.; Tong, Z. Kinetics and Products of the Reactions of Nitrate Radical with Monoalkenes, Dialkenes, and Monoterpenes. *J. Phys. Chem.* **1990**, *94*, 2413−2419.
(41) Skov, H.; Hjorth, J.; Lohse, C.; Jensen, N. R.; Restelli, G. Products and Mechanisms of the Reactions of the Nitrate Radical (NO_3) with Isoprene, 1,3-Butadiene and 2,3-Dimethyl-1,3-Butadiene in Air. *Atmos. Environ., Part A* **1992**, *26*, 2771−2783.
(42) Skov, H.; Benter, T.; Schindler, R. N.; Hjorth, J.; Restelli, G. Epoxide Formation in the Reactions of the Nitrate Radical with 2,3-Dimethyl-2-Butene, Cis- and Trans-2-Butene and Isoprene. *Atmos. Environ.* **1994**, *28*, 1583−1592.
(43) Kwok, E. S. C.; Aschmann, S. M.; Arey, J.; Atkinson, R. Product Formation from the Reaction of the NO_3 Radical with Isoprene and Rate Constants for the Reactions of Methacrolein and Methyl Vinyl Ketone with the NO_3 Radical. *Int. J. Chem. Kinet.* **1996**, *28*, 925−934.
(44) Perring, A. E.; Wisthaler, A.; Graus, M.; Wooldridge, P. J.; Lockwood, A. L.; Mielke, L. H.; Shepson, P. B.; Hansel, A.; Cohen, R. C. A Product Study of the Isoprene + NO_3 Reaction. *Atmos. Chem. Phys.* **2009**, *9*, 4945−4956.
(45) Kwan, A. J.; Chan, A. W. H.; Ng, N. L.; Kjaergaard, H. G.; Seinfeld, J. H.; Wennberg, P. O. Peroxy Radical Chemistry and OH Radical Production during the NO_3 -Initiated Oxidation of Isoprene. *Atmos. Chem. Phys.* **2012**, *12*, 7499−7515.
(46) Vereecken, L.; Carlsson, P.; Bernard, F.; Brown, S. S.; Cho, C.; Friedrich, N.; Fuchs, H.; Liebmann, J. M.; Mellouki, W.; Novelli, A.; Reimer, D.; Tillmann, R.; Zhou, L.; Kiendler-Scharr, A.; Wahner, A. Theoretical and Experimental Study of Peroxy and Alkoxy Radicals in the NO_3-Initiated Oxidation of Isoprene. *Phys. Chem. Chem. Phys.* **2021**, DOI: 10.1039/d0cp06267g. , accepted
(47) Pye, H. O. T.; Luecken, D. J.; Xu, L.; Boyd, C. M.; Ng, N. L.; Baker, K. R.; Ayres, B. R.; Bash, J. O.; Baumann, K.; Carter, W. P. L.; Edgerton, E.; Fry, J. L.; Hutzell, W. T.; Schwede, D. B.; Shepson, P. B. Modeling the Current and Future Roles of Particulate Organic Nitrates in the Southeastern United States. *Environ. Sci. Technol.* **2015**, *49*, 14195−14203.
(48) Darer, A. I.; Cole-Filipiak, N. C.; O'Connor, A. E.; Elrod, M. J. Formation and Stability of Atmospherically Relevant Isoprene-Derived Organosulfates and Organonitrates. *Environ. Sci. Technol.* **2011**, *45*, 1895−1902.
(49) Hu, K. S.; Darer, A. I.; Elrod, M. J. Thermodynamics and Kinetics of the Hydrolysis of Atmospherically Relevant Organonitrates and Organosulfates. *Atmos. Chem. Phys.* **2011**, *11*, 8307−8320.
(50) Takeuchi, M.; Ng, N. L. Chemical Composition and Hydrolysis of Organic Nitrate Aerosol Formed from Hydroxyl and Nitrate Radical Oxidation of α -Pinene and β -Pinene. *Atmos. Chem. Phys.* **2019**, *19*, 12749−12766.
(51) Vasquez, K. T.; Crounse, J. D.; Schulze, B. C.; Bates, K. H.; Teng, A. P.; Xu, L.; Allen, H. M.; Wennberg, P. O. Rapid hydrolysis of tertiary isoprene nitrate efficiently removes NOx from the atmosphere. *Proc. Natl. Acad. Sci. U.S.A.* **2020**, *117*, 33011−33016.
(52) Zaveri, R. A.; Shilling, J. E.; Fast, J. D.; Springston, S. R. Efficient Nighttime Biogenic SOA Formation in a Polluted Residual Layer. *J. Geophys. Res.: Atmos.* **2020**, *125*, No. e2019JD031583.
(53) Pankow, J. F.; Asher, W. E. SIMPOL.1: A Simple Group Contribution Method for Predicting Vapor Pressures and Enthalpies of Vaporization of Multifunctional Organic Compounds. *Atmos. Chem. Phys.* **2008**, *8*, 2773−2796.
(54) Wu, R.; Vereecken, L.; Tsiligiannis, E.; Kang, S.; Albrecht, S. R.; Hantschke, L.; Zhao, D.; Novelli, A.; Fuchs, H.; Tillmann, R.; Hohaus, T.; Carlsson, P.; Shenolikar, J.; Bernard, F.; Crowley, J. N.; Fry, J. L.; Brownwood, B.; Thornton, J. A.; Brown, S. S.; Kiendler-Scharr, A.; Wahner, A.; Hallquist, M.; Mentel, T. F. Molecular Composition and Volatility of Multi-Generation Products Formed from Isoprene Oxidation by Nitrate Radical. *Atmos. Chem. Phys.* **2020**, under review.